
Explicitly Modeling Generality into Self-Supervised Learning

Jingyao Wang^{1,2} Wenwen Qiang^{1,2} Changwen Zheng^{1,2}

Abstract

The goal of generality in machine learning is to achieve excellent performance on various unseen tasks and domains. Recently, self-supervised learning (SSL) has been regarded as an effective method to achieve this goal. It can learn high-quality representations from unlabeled data and achieve promising empirical performance on multiple downstream tasks. Existing SSL methods mainly constrain generality from two aspects: (i) large-scale training data, and (ii) learning task-level shared knowledge. However, these methods lack explicit modeling of the SSL generality in the learning objective, and the theoretical understanding of SSL’s generality remains limited. This may cause SSL models to overfit in data-scarce situations and generalize poorly in the real world, making it difficult to achieve true generality. To address these issues, we provide a theoretical definition of generality in SSL and define a σ -measurement to help quantify it. Based on this insight, we explicitly model generality into self-supervised learning and further propose a novel SSL framework, called GeSSL. It introduces a self-motivated target based on σ -measurement, which enables the model to find the optimal update direction towards generality. Extensive theoretical and empirical evaluations demonstrate the superior performance of the proposed GeSSL.

1. Introduction

The goal of generality in machine learning is to handle various unseen tasks well (McCarthy, 1987; Risi & Togelius, 2020). Recently, self-supervised learning (SSL) has been considered a promising approach to achieve this goal, since it achieves great performance in various scenarios without

supervision (Krishnan et al., 2022; Schiappa et al., 2022).

SSL performs learning by applying various data augmentations and encouraging the augmented views of the same sample closer while pushing apart views from other samples, and then uses the learned knowledge to solve new tasks (Shurrab & Duwairi, 2022; Baevski et al., 2022). This learning process constrains the SSL models to be more general from two aspects: (i) data level: learning based on a large amount of data and various data augmentation methods, making the model acquire rich knowledge (Ericsson et al., 2022); and (ii) learning paradigm level: treating different batches as different tasks, making the model obtain task-level shared information (Ni et al., 2021). However, existing SSL models neglect the explicit modeling of the generality in their objectives, and the relevant theoretical understanding remains insufficient, making the SSL models still difficult to achieve generality in real-life applications (Huang et al., 2021; Sun et al., 2020; Ericsson et al., 2022).

To address this issue, we aim to explicitly model generality into SSL’s objective in this study. We solve the following two problems: (i) *how to define the generality of SSL models*, and (ii) *how to ensure the generality of SSL models*.

For the first problem, we begin by understanding the manifestation of generality in SSL, finding that the generality can be reflected in two aspects (Huang et al., 2021; Shen et al., 2021): learning generality and evaluation generality. The former aims to make the model learn general representations for various samples of each task during training, while the latter aims to make the model achieve excellent performance on various downstream tasks. Based on the above discussion, we give the mathematical definition of the generality and propose a σ -measurement to help quantify it. This definition involves discriminability, transferability, and generalization at the same time, which can be used in all SSL paradigms. We further provide theoretical support and performance guarantees for the proposed definition.

Based on this insight, for the second problem, we explicitly model generality into SSL. Specifically, we first regard the augmented data in a single batch as a multi-class classification task (see Subsection 3.2). Then, we use bi-level optimization to constrain the model to learn a general representation for multiple tasks based on σ -measurement. In the first level, we make the model quickly adapt to each

¹Institute of Software Chinese Academy of Sciences, Beijing, China ²University of the Chinese Academy of Sciences, Beijing, China. Correspondence to: Wenwen Qiang <a01114115@163.com>.

training task with the representation learned before; in the second level, we constrain the model to achieve comparative performance on various tasks with the learned representations through a σ -measurement-based self-motivated target. The targets correspond to learning and evaluation generality respectively, constraining the model to update in the optimal direction towards generality.

Our contributions: (i) We are the first to explore direct modeling of generality into SSL. (ii) We theoretically define the generality of SSL and propose a σ -measurement to help quantify it. (iii) We explicitly model the generality into the SSL objective and propose a novel SSL framework, called GeSSL. It updates through a bi-level optimization guided by the proposed self-motivated target, which enables the model to update along the optimal direction towards generality. (iv) We conduct theoretical and empirical evaluations on various downstream scenarios, demonstrating the superior robustness and generalization of GeSSL.

2. Related Work

2.1. Self-supervised Learning

SSL methods provide a powerful representation by transferring knowledge from pretext tasks without the need for annotations. Following (Jaiswal et al., 2020; Kang et al., 2023), existing SSL methods mainly can be divided into five types, including (i) learning similar representations for each sample by perturbing it with data augmentation, while learning discriminative representations with data augmented from other samples, e.g., SimCLR (Chen et al., 2020a) and MoCo v2 (Chen et al., 2020b); (ii) similar to (i), which also learn representations from different augmented views, but do not rely on negative pairs, e.g., BYOL (Grill et al., 2020), SimSiam (Chen & He, 2021), Barlow Twins (Zbontar et al., 2021), and VicReg (Bardes et al., 2022); (iii) using the concept of clustering to distinguish clusters of representations instead of explicit sample pairs, e.g., DeepCluster (Caron et al., 2018) and SwAV (Caron et al., 2020); (iv) attempt to investigate techniques that facilitate SSL under ViT-based architectures (Dosovitskiy et al., 2020), e.g., SiT (Atito et al., 2021), DINO (Caron et al., 2021) and EsViT (Li et al., 2021a), which have proven their effectiveness in various tasks; and (v) generative-based SSL that learn data distributions to generate new and similar samples, e.g., MAE (Hou et al., 2022), GeSimCLR (Mohamed et al., 2022). In this study, we investigate the generality of SSL and propose a model-agnostic framework that explicitly models generality into the learning objective and can be applied across any SSL model, including all five types of methods.

2.2. Generality in Self-supervised Learning

SSL emerged as a powerful technique in the field of unsupervised representation learning. SSL methods learn general representations to achieve good generalization while avoiding the cost of labeling large-scale data sets (Schiappa et al., 2022; Baevski et al., 2022). However, despite the empirical effectiveness of SSL methods that have been proven, they still face various challenges (Jaiswal et al., 2020), making it difficult for the models to be truly general. For example, SSL models generalize poorly (i) when data are scarce (Krishnan et al., 2022), or (ii) in real-life applications that have a lot of noise (Goyal et al., 2021). Moreover, SSL models result in overfitting or underfitting when facing semantic inconsistency or ambiguous data (Araslanov & Roth, 2021; Li et al., 2020), e.g., the object orientation in rotation prediction is not fixed. In addition, the performance of SSL models is affected by the matching between pretext and downstream tasks, and may be difficult to transfer well (Tendle & Hasan, 2021). These situations will cause obstacles to the generality of the SSL models (Huang et al., 2021). The experiments described in Section 6 and Appendix F further demonstrate the limitations of existing SSL methods. In this study, we explore how to achieve the generality of SSL and explicitly model it into the objective to unleash its potential.

3. Preliminary

In this section, we first introduce the primary paradigm of self-supervised learning. Next, we describe the process of self-supervised task construction, i.e., treating a single batch of self-supervised learning as a classification task.

3.1. Self-supervised Learning

Given a dataset $\mathcal{D} = \{x_i\}_{i=1}^N$ and a data augmentations distribution $\mathcal{A} = \{a^j(x_i)\}_{i=1, j=1}^{N, 2}$, the SSL model are denoted as $f_\theta = h \circ g$ with a feature extractor $g(\cdot)$ and a projection head $h(\cdot)$. The feature extractor $g(\cdot)$ is structured as a backbone neural network, and the projection head $h(\cdot)$ can be realized as a multi-layer perceptron (MLP) or a single-layer weight matrix. Then, the SSL objective can be written as:

$$\min_{f_\theta} \mathcal{L}_{\text{SSL}}(f_\theta; \mathcal{D}, \mathcal{A}) := \mathbb{E}_{\mathcal{B}_x \sim \mathcal{D}}[\ell(f_\theta; \mathcal{Z}_x)] \quad (1)$$

where $z_{x_i}^j = h(g(a^j(x_i))) = f_\theta(a^j(x_i)) \in \mathcal{Z}_x$ denotes the embedding of $a^j(x_i)$, where $\mathbf{x} = \{x_i\}_{i=1}^B \in \mathcal{B}_x$ are the data in a mini-batch $\mathcal{B}_x \in \mathcal{D}$. Note that the $\ell(\cdot)$ can be the loss functions for any SSL paradigms, e.g., for contrastive SSL, $\ell(\cdot)$ is the InfoNCE loss:

$$\ell(f_\theta; \mathcal{Z}_x) = - \sum_{z_{x_i}^j \in \mathcal{Z}_x} \log \frac{\exp(\cos(z_{x_i}^j, z_{x_i}^{3-j})/\tau)}{\sum_{z_{x_i}^j \in \mathcal{Z}_x} \exp(\cos(z_{x_i}^j, z_{x_i})/\tau)} \quad (2)$$

where $\cos(\mathbf{u}, \mathbf{v}) = \mathbf{u}^T \mathbf{v} / \|\mathbf{u}\| \|\mathbf{v}\|$, τ is a hyperparameter for temperature scaling. Given the sample x_i , $z_{x_i}^j$ is the

embedding of the anchor, and $z_{x_i}^{3-j}$ is the embedding of the positive sample related to the anchor, where j and $3-j$ refer to the indexes of samples, e.g., when $j = 1$, the notation of another augmented sample is $3-j = 2$. The goal of Eq.2 is to maximize the similarity between $z_{x_i}^j$ and $z_{x_i}^{3-j}$, while simultaneously minimizing the similarities between $z_{x_i}^j$ and the embeddings of negative samples $\mathcal{Z}_x \setminus \{z_{x_i}^j, z_{x_i}^{3-j}\}$.

After training, the projection head $h(\cdot)$ is no longer used, and the trainable weights in the feature extractor $g(\cdot)$ are frozen. A coefficient matrix $\mathcal{W} \subseteq \mathbb{R}^{n \times d}$ is trained using the training set \mathcal{D}_{tr}^{ds} of the downstream task, where n and d are the number and the embedding dimension of the samples. The performance of f_θ on the downstream task can be assessed using maximum likelihood estimation (MLE) on the test set \mathcal{D}_{te}^{ds} , as described below:

$$\begin{aligned} \mathcal{L}_{ds}(\mathcal{W}; f_\theta, \mathcal{D}_{te}^{ds}, \mathcal{D}_{tr}^{ds}) &= \mathbb{E}_{(x,y) \sim \mathcal{D}_{te}^{ds}} [-\log P(y; \mathcal{W}f_\theta(x))] \\ \text{s.t. } \mathcal{W} &= \arg \max_{\mathcal{W}} \mathbb{E}_{(x,y) \sim \mathcal{D}_{tr}^{ds}} [\log P(y; \mathcal{W}f_\theta(x))] \end{aligned} \quad (3)$$

3.2. Self-supervised Task Construction

We now describe how to construct SSL tasks. Following (Araslanov & Roth, 2021), as there is significant entity similarity in data augmented from the same image, we assign the same label $y_i \in \mathcal{Y}$ to the augmented data of the same image x_i , i.e., one batch of SSL can be regarded as a multi-class classification task, with each class containing two samples. The theoretical evaluation is provided in Section 5.

Formally, given the data of the mini-batch \mathcal{B}_x , each anchor x_i and its augmented sample (positive) $a^j(x_i)$ have the same label, denoted as y_i . Then the dataset of \mathcal{B}_x can be represented as $\mathcal{D}_x = (\mathcal{X}, \mathcal{Y})$ where $\mathcal{X} = \{a^j(x_i)\}_{i=1, j=2}^{i=B, j=2}$ and $\mathcal{Y} = \{y_i\}_{i=1}^B$ denote the samples and the corresponding labels. The learning of \mathcal{B}_x constitutes a B -class classification task, and each class contains two samples $a^1(x_i)$ and $a^2(x_i)$ with label y_i . We stick f_θ as the classifier, then Eq.2 can be regarded as a softmax function and expressed as a probability distribution:

$$\ell(f_\theta; \mathcal{D}_x) = - \sum_{a^j(x_i) \in \mathcal{D}_x} \log P(y_i, f_\theta(a^j(x_i))) \quad (4)$$

Eq.4 indicates that the learning objective turns to learning a task-agnostic model f_θ^* that applies well to all tasks. Note that we add a classification head after the projection head in the network to provide structural support.

4. Method

In this section, we first analyze the manifestation of generality in SSL and give a mathematical definition with theoretical support. Next, we propose the σ -measurement to

help quantify generality. Finally, we propose a novel SSL framework (GeSSL) to explicitly model generality in SSL.

4.1. Definition of Generality

The generality of SSL can be reflected in two aspects (Huang et al., 2021; Shen et al., 2021), i.e., learning generality and evaluation generality. They can be explained from the training stage and the testing stage respectively: (i) learning generality, i.e., the model f_θ which learns general representations during the training stage, should achieve comparable performance on each task quickly with few data; (ii) evaluation generality, i.e., the trained f_θ^* , which has learned general representations, should adapt to different tasks simultaneously with minimal additional data, i.e., few-shot or zero-shot. In other words, if the trained model learns general knowledge well, it should perform well on each task, approaching the task-specific optimal model for each task.

Based on this insight, we consider a single batch of SSL as a multi-class classification task as mentioned in Subsection 3.2, and give a definition of the generality of SSL.

Definition 4.1. (Generality of SSL) *The SSL model $f_\theta = h \circ g$ is said to exhibit generality if, for any set of training tasks $\mathcal{T}^{tr} = \{\mathcal{T}_i^{tr}\}_{i=1}^N$ and target tasks $\mathcal{T}^{te} = \{\mathcal{T}_k^{te}\}_{k=1}^M$ without class-level overlap, the following conditions hold:*

For training tasks \mathcal{T}^{tr} , the model f_θ trained on task \mathcal{T}_i^{tr} can achieve competitive performance quickly on task \mathcal{T}_j^{tr} through few samples $\mathcal{D}_i^{tr} = (\mathcal{X}_i^{tr}, \mathcal{Y}_i^{tr})$.

For target tasks \mathcal{T}^{te} , the trained model f_θ^ can achieve comparable performance with all the optimal task-specific models on all the target tasks through minimal additional data $\mathcal{D}_{min}^{te} = \{\mathcal{D}_k^{te}\}_{k=1}^M$, where $\mathcal{D}_k^{te} = (\mathcal{X}_k^{te}, \mathcal{Y}_k^{te})$.*

This definition imposes the two constraints of the SSL generality mentioned above, i.e., learning generality and evaluation generality, which involve discriminability, transferability, and generalization. In brief, learning generality requires the model to achieve great performance on different samples of each task with the learned representation during training (discriminability), while also meaning that the model based on the representations learned on other tasks can adapt well to the current task with few samples (transferability). Evaluation generality requires that the trained model can achieve good results on various target tasks based on the learned general representation (generalization).

For the differences and relation of learning and evaluation generality: (i) Their differences lie in that learning generality refers to the rapid adaptation of the model to each specific task during training, referring to discriminability and transferability, while evaluation generality refers to the performance of the trained model in various tasks, referring to generalization. Their differences are reflected in the two

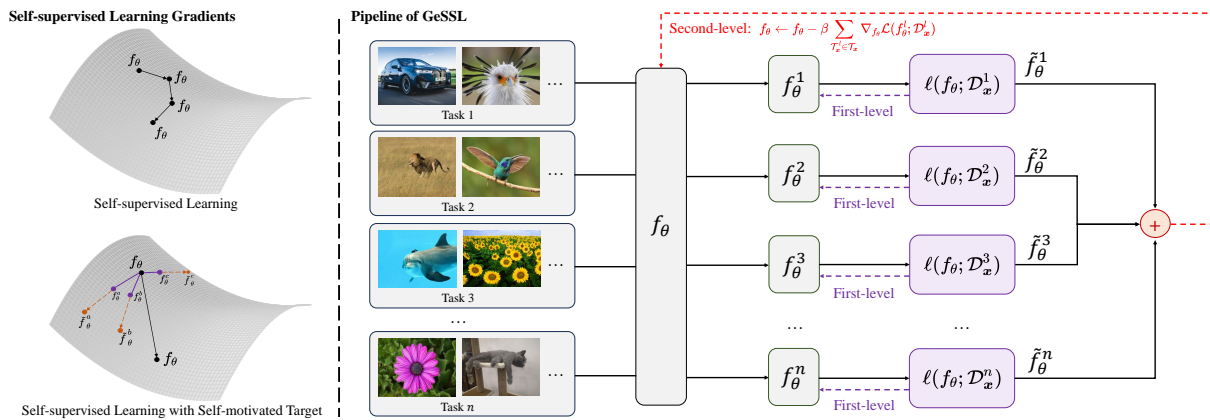


Figure 1. An overview of GeSSL and the learning gradients. Each SSL task is introduced as a batch of SSL with multiple classes, and each class includes a pair of positive examples augmented from the same sample. The purple dashed line refers to the first-level optimization that performs gradient descent on performance on each batch/task directly, while the red dashed line refers to the second-level optimization that incentive moving in loss curve toward target minima for multiple tasks. The **pseudo-code** is provided in Appendix A.

stages of training vs. evaluation, and the performance of each single task vs. all tasks. (ii) Their relation lies in that they cover all stages of model learning and evaluation, and jointly require the model to be close to generality.

Compared to previous works that focus on the general representations of SSL (Eastwood et al., 2023; Balazevic et al., 2024) or the generalization (Hsu et al., 2018; Ni et al., 2021), the generality studied in this paper is a more fundamental and rigorous concept for three reasons: (i) It is defined from both learning and evaluation generality and constrain the discriminability, transferability, and generalization of SSL, while the previous works only focused on generalization. (ii) The previous works focused either on the performance of unseen samples of the related domains, i.e., supervised learning (Shahrampour et al., 2018) or domain generalization (Li et al., 2017), or different tasks, i.e., meta-learning (Hsu et al., 2018; Ni et al., 2021), while the generality in this paper requires the model effect on both different samples and tasks which contains both the meanings.

4.2. Measurement of Generality

According to Definition 4.1, the necessary and sufficient condition for the SSL generality is that the model can learn general representations, and adapt well to downstream tasks, thereby reducing the error rate. Based on this, we propose the σ -measurement to help quantify the generality. Specifically, $\sigma(f_\theta^*)$ measures the performance gap between the trained model f_θ^* and the task-specific optimal model $f_{\phi_i}^*$ (ground-truth with 100% accuracy) on various downstream tasks. In other words, the more general representation learned by f_θ^* that can capture high-level features, the closer the effect on downstream tasks is to $f_{\phi_i}^*$.

Definition 4.2. (σ -measurement) Given a set of unseen test

tasks $\mathcal{T}^{te} = (\mathcal{X}^{te}, \mathcal{Y}^{te})$, assume that the optimal parameter θ^* is independent of \mathcal{X}^{te} , i.e., not change due to the distribution of test tasks, and the covariance of θ^* satisfies $\text{Cov}[\theta^*] = (R^2/d)\mathcal{I}_d$, where R is a constant, d is the dimension of the model parameter, and \mathcal{I}_d is a identity matrix, the error rate $\sigma(f_\theta^*)$ is:

$$\sigma(f_\theta^*) = \sum_{\mathcal{T}_i^{te} \in \mathcal{T}^{te}} \mu_{KL}(\pi_{f_\theta^*}, \pi_{f_{\phi_i}^*}) \quad (5)$$

where $\mu_{KL}(p||q) = \int p(x) \log \left(\frac{p(x)}{q(x)} \right) dx$ is the calculation of Kullback-Leibler Divergence which is estimated via variational inference, $\pi_{f_\theta^*}$ and $\pi_{f_{\phi_i}^*}$ are the output probabilistic distributions of the trained model f_θ^* and the task-specific optimal model $f_{\phi_i}^*$ on task \mathcal{T}_i^{te} .

We provide the performance guarantee of using the σ -measurement in self-supervised models in Section 5, which provides theoretical support for our definition. This measurement directly inspires the design of the second-level optimization objective. Meanwhile, we conduct experiments for generality evaluation in Appendix F.3. Combining the results in Section 6, the results demonstrate that existing SSL models have limited generality, and the generality performance improvement brought by GeSSL is stably achieved.

4.3. Explicit Modeling of Generality

Based on the above insight, we explicitly model generality into self-supervised learning and propose a novel SSL framework as shown in Figure 1, called GeSSL. It learns general knowledge through a bi-level optimization over a set of SSL tasks conducted as described in Subsection 3.2. Note that the objectives of the bi-level optimization process are directly inspired by the learning and evaluation generality defined in Definition 4.1. GeSSL can be integrated into any

SSL model to explicitly model the generality of the model.

For the first level, the SSL model $f_\theta = h \circ g$ aims to learn task-specific knowledge by minimizing the loss ℓ over each SSL task with limited update steps. It corresponds to the learning generality, which constrains the model f_θ to update a few steps on each task, obtaining multiple task-specific models f_θ^l that always achieve great performance during training. Then, the objective can be expressed as:

$$\begin{aligned} f_\theta^l &\leftarrow f_\theta - \alpha \nabla_{f_\theta} \ell(f_\theta; \mathcal{D}_x^l) \\ \text{s.t. } \ell(f_\theta; \mathcal{D}_x^l) &= - \sum_{a^j(x_i^l) \in \mathcal{D}_x^l} \log P(y_i^l, f_\theta(a^j(x_i^l))) \end{aligned} \quad (6)$$

where α denotes the learning rate, f_θ^l denotes the SSL model learned through K steps ($K = 1$ corresponds to the required "quickly") over task \mathcal{T}_x^l (also the l -th training batch \mathcal{B}_x^l), $\mathcal{D}_x^l = (\mathcal{X}^l, \mathcal{Y}^l)$ denotes the training data of SSL task \mathcal{T}_x^l , where $\mathcal{X}^l = \{a^j(x_i^l)\}_{i=1, j=2}^{i=B, j=2}$ and $\mathcal{Y}^l = \{y_i^l\}_{i=1}^B$ are the samples and the corresponding labels. All the SSL tasks are conducted as mentioned in Subsection 3.2. Considering that f_θ^l is obtained by one update of f_θ , it actually evaluates the performance of f_θ . In a specific round of training, when the model f_θ is based on just one step update on each task of the current batch, the effect of f_θ^l and better \tilde{f}_θ^l is almost the same (KL divergence loss ≈ 0 in the second-level), then it is considered that the model approaches evaluation generality.

For the second level, the SSL model f_θ aims to further refine the learned representations, so as to capture the general knowledge across various SSL tasks. This level corresponds to the evaluation generality, which constrains the model f_θ from adapting to different tasks and domains with the learned general representations.

Specifically, inspired by the σ -measurement, we propose that the trained f_θ that learns the general knowledge should be close to the task-specific optimal model $f_{\phi_i}^*$ on each task.

Based on this insight, we design a self-motivated target $\tilde{f}_\theta^l = \delta(f_\theta^l)$, where the policy δ performs $\lambda - 1$ steps of updates further on the task \mathcal{T}_x^l before taking the final gradient step for each model f_θ^l in the first-level optimization, obtaining \tilde{f}_θ^l . The model \tilde{f}_θ^l is considered to be more sufficiently updated and closer to the $f_{\phi_i}^*$ than f_θ^l . Next, by constraining f_θ to approach the self-motivated target \tilde{f}_θ^l on each task, we encourage the model to follow the optimal path and achieve the optimal state faster and better. Then, the objective of the second-level optimization can be expressed as:

$$\begin{aligned} f_\theta &\leftarrow f_\theta - \beta \sum_{\mathcal{T}_x^l \in \mathcal{T}_x} \nabla_{f_\theta} \mathcal{L}(f_\theta^l; \mathcal{D}_x^l) \\ \text{s.t. } \mathcal{L}(f_\theta^l; \mathcal{D}_x^l) &= \mu_{KL}(\pi_{\tilde{f}_\theta^l}, \pi_{f_\theta^l}) \end{aligned} \quad (7)$$

where β is the learning rate, $\mu(\cdot|\cdot)$ denotes Kullback-Leibler Divergence as mentioned in Definition 4.2, $\pi_{\tilde{f}_\theta^l}$ and $\pi_{f_\theta^l}$ are the probabilistic distributions of \tilde{f}_θ^l and f_θ^l .

In summary, at the first level, we constrain the model to learn task-specific representations, so that it achieves good performance on each task. At the second level, we constrain the model to further refine the learned representations, so that it obtains general knowledge and achieves good performance on all tasks. The closed form mathematical objective of the bi-level optimization can be expressed as:

$$\begin{aligned} \arg \min_{f_\theta} \sum_{\mathcal{T}_x^l \in \mathcal{T}_x} \mathcal{L}(f_\theta^l; \mathcal{D}_x^l) \\ \text{s.t. } f_\theta^l = \arg \min_{f_\theta} \ell(f_\theta; \mathcal{D}_x^l) \end{aligned} \quad (8)$$

Thus, we explicitly model generality into the objective of self-supervised learning.

5. Theoretical Evaluation

In this section, we first prove the rationality of the task construction in Subsection 3.2. Next, we analyze the performance guarantee of GeSSL that is conducted based on Definition 4.1 and 4.2. We defer all proofs to Appendix B.

First, consider task construction described in Section 3.2, the goal is to identify a representation that allows us to approximate different "reasonable" choices by f_θ . It can group augmented views of similar entities together, i.e. every SSL model f_θ that satisfies:

Theorem 5.1. (Approximate View-Invariance): *The best estimate of the label y is approximately invariant to the choice of different augmented views $a^j(x)$, $j = 1, 2$ of the same x . Each target function $f_\theta : \mathcal{A} \rightarrow \mathbb{R}^n$ satisfies:*

$$\mathbb{E}_{p_+(a^1(x), a^2(x))} [(f_\theta(a^1(x)) - f_\theta(a^2(x)))^2] \leq \varepsilon \quad (9)$$

where $p_+(a^1(x), a^2(x)) = \sum_x p(a^1(x)|x)p(a^2(x)|x)p(x)$ when fixed $\varepsilon \in [0, \infty)$.

We can then constrain the error of approximating f_θ with a small subset of eigenfunctions, making each coefficient according to its contribution to the total positive pair difference. We focus on a class of linear predictors on top of k -dimensional representations $r : \mathcal{A} \rightarrow \mathbb{R}^n$, among which the best choice used for task-specific training (Eq.6) is the representation $r^d = \{p_1(a(x)), \dots, p_d(a(x))\}$. This representation r^d contains d eigenfunctions of the positive-pair Markov chain with the largest eigenvalues.

Next, we turn to the performance guarantee of GeSSL. We restrict our attention to the noise-less setting (true expectation) and analyze how the performance around f_θ^l changes by updating f_θ . We assume that the output of μ_{KL} is differentiable and convex with a minimum value of 0.

Theorem 5.2. (Performance Guarantee) *Let \tilde{f}_θ^l and f_θ^l be SSL models before and after learning general knowledge based on Eq.7, $\mu_{KL}^f(\theta_1, \theta_2) = \mu_{KL}(\pi_{\tilde{f}_\theta^l}, \pi_{f_\theta^l})$ is similar*

to Kullback-Leibler Divergence but with gradient calculation, the update process for each task satisfies:

$$\begin{aligned} \tilde{f}_\theta - f_\theta &= \frac{\beta}{\alpha} \mu_{KL}^f(\tilde{f}_\theta^l, f_\theta^l - \alpha \mathcal{G}^T g) \\ &\quad - \frac{\beta}{\alpha} \mu_{KL}^f(\tilde{f}_\theta^l, f_\theta^l) + o(\beta(\alpha + \beta)) \end{aligned} \quad (10)$$

where $\mathcal{G}^T = \mathcal{M}^T \mathcal{M} \in \mathbb{R}^{n_\theta \times n_\theta}$ with the (transposed) Jacobian \mathcal{M} of f_θ^l , i.e., $\mathcal{M} := \left[\frac{\partial \theta^l}{\partial \theta} \right] \in \mathbb{R}^{n_{\theta^l} \times n_\theta}$. Note that $\nabla_{f_\theta} f_\theta^l = \mathcal{M} \nabla_{f_\theta^l} f_\theta^l$. When β sufficiently small, there exists infinitely many σ for which $\tilde{f}_\theta - f_\theta \leq 0$. The self-motivated target σ yields improvements

$$\tilde{f}_\theta - f_\theta = -\frac{\beta}{\alpha} \mu_{KL}^f(\tilde{f}_\theta^l, f_\theta^l) + o(\beta(\alpha + \beta)) \leq 0 \quad (11)$$

Compared to standard self-supervised (learning f_θ from scratch with single optimization), our method enables the model f_θ to reach optimal results faster while achieving convergence without utilizing gradient updates. The proof and more analysis are provided in Appendix B. Meanwhile, (Mohri et al., 2018; Bansal et al., 2020) proves that as training progresses, the tasks learned by the model will be distributed in a wider manifold space, and their correlation with test tasks will become stronger. Similarly, with the training of model f_θ , the learned representation becomes more effective since it learns from more diverse tasks, and the correlation of downstream tasks with training tasks is getting stronger. More details are provided in the Appendix.

6. Empirical Evaluation

In this section, we first introduce the datasets in Subsection 6.1. Next, we conduct experiments on multiple scenarios for evaluation in Subsections 6.2-6.5, including unsupervised learning, semi-supervised learning, transfer learning, and few-shot learning. We introduce the experimental setups in the corresponding sections. More details are provided in Appendix C. Finally, we perform ablation studies in Subsection 6.6. All results reported are the averages of five independent runs and performed on NVIDIA RTX 4090 GPUs. More experiments are shown in Appendix F and G due to space limitations. All experimental results demonstrate the superior effectiveness, robustness, and efficiency of GeSSL in various fields and modalities, e.g., instance segmentation, video tracking, image generation, text recognition, etc.

6.1. Benchmark Datasets

For unsupervised learning, we use six benchmark datasets for evaluation, including CIFAR-10 (Krizhevsky et al., 2009), CIFAR-100 (Krizhevsky et al., 2009), STL-10 (Coates et al., 2011), Tiny ImageNet (Le & Yang, 2015), ImageNet-100 (Tian et al., 2020) and ImageNet (Deng et al., 2009). For semi-supervised learning, we evaluate GeSSL

on ImageNet (Deng et al., 2009). For transfer learning, we mainly select two scenarios: instance segmentation (PASCAL VOC (Everingham et al., 2010)) and object detection (COCO (Lin et al., 2014)) for analysis. For few-shot learning, we select three benchmarks, including Omniglot (Lake et al., 2019), miniImageNet (Vinyals et al., 2016a), and CIFAR-FS (Bertinetto et al., 2018). More details are provided in Appendix D.

6.2. Unsupervised Learning

Experimental setup. We adopt the most commonly used protocol for SSL (Chen et al., 2020a), freezing the feature extractor and training a supervised linear classifier on top of it. We use the Stochastic Gradient Descent (SGD) optimizer with a momentum of 0.9 to optimize our objectives. The linear classifier runs for 500 epochs with a batch size of 128 and a learning rate that starts at 5×10^{-2} , and decays to 5×10^{-6} until the training is completed. We use ResNet-18 as the feature extractor for small-scale datasets, i.e., CIFAR-10, CIFAR-100, STL-10, and Tiny ImageNet, while using ResNet-50 for the medium-scale dataset, i.e., ImageNet-100, and the large-scale dataset, i.e., ImageNet. The λ of the self-motivated target policy δ is set to 10.

Results. Table 1 shows the results on four small-scale datasets. We can observe that applying the proposed GeSSL framework significantly outperforms the state-of-the-art (SOTA) methods on all four datasets. Moreover, applying our GeSSL framework to all four types of representative SSL models as described in Subsection 2.1, including SimCLR, MoCo, BYOL, Barlow Twins, SwAV, and DINO, achieves an average improvement of 3% compared to the original frameworks. Table 2 shows the top-1 and top-5 linear classification accuracies on ImageNet-100 and ImageNet. Our GeSSL framework still surpasses other SOTA methods, demonstrating its ability to enhance the performance of self-supervised learning methods. The full results with different epochs are provided in Appendix F.1.

6.3. Semi-supervised Learning

Experimental setup. We adopt the commonly used protocol for semi-supervised learning (Zbontar et al., 2021). We create two balanced subsets by sampling 1% and 10% of the training dataset. We fine-tune the models on these two subsets for 50 epochs with different learning rates for the classifier and the backbone network. Specifically, we use 0.05 and 1.0 for the classifier, and 0.0001 and 0.01 for the backbone, on the 1% and 10% subsets, respectively. The λ of the self-motivated target policy δ is set to 10 with $K = 1$.

Results. Table 3 shows the semi-supervised learning results on ImageNet. We can observe that the performance after applying our GeSSL is superior to the SOTA methods. Specifically, when only 1% of the labels are available in

Submission and Formatting Instructions for ICML 2024

Table 1. The classification accuracies ($\pm 95\%$ confidence interval) of a linear classifier (linear) and a 5-nearest neighbors classifier (5-nn) with a ResNet-18 as the feature extractor. The comparison baselines cover almost all types of methods mentioned in Subsection 2.1. The “-” denotes that the results are not reported. More details of the baselines are provided in Appendix E.

Method	CIFAR-10		CIFAR-100		STL-10		Tiny ImageNet	
	linear	5 - nn	linear	5 - nn	linear	5 - nn	linear	5 - nn
SimCLR (Chen et al., 2020a)	91.80 \pm 0.15	88.42 \pm 0.15	66.83 \pm 0.27	56.56 \pm 0.18	90.51 \pm 0.14	85.68 \pm 0.10	48.84 \pm 0.15	32.86 \pm 0.25
MoCo (Chen et al., 2020b)	91.69 \pm 0.12	88.66 \pm 0.14	67.02 \pm 0.16	56.29 \pm 0.25	90.64 \pm 0.28	88.01 \pm 0.19	50.92 \pm 0.22	35.55 \pm 0.16
BYOL (Grill et al., 2020)	91.93 \pm 0.22	89.45 \pm 0.22	66.60 \pm 0.16	56.82 \pm 0.17	91.99 \pm 0.13	88.64 \pm 0.20	51.00 \pm 0.12	36.24 \pm 0.28
SimSiam (Chen & He, 2021)	91.71 \pm 0.27	88.65 \pm 0.17	67.22 \pm 0.26	56.36 \pm 0.19	91.01 \pm 0.19	88.16 \pm 0.19	51.14 \pm 0.20	35.67 \pm 0.16
Barlow Twins (Zbontar et al., 2021)	90.88 \pm 0.19	89.68 \pm 0.21	66.13 \pm 0.10	56.70 \pm 0.25	90.38 \pm 0.13	87.13 \pm 0.23	49.78 \pm 0.26	34.18 \pm 0.18
SwAV (Caron et al., 2020)	91.03 \pm 0.19	89.52 \pm 0.24	66.56 \pm 0.17	57.01 \pm 0.25	90.72 \pm 0.29	86.24 \pm 0.26	52.02 \pm 0.26	37.40 \pm 0.11
DINO (Caron et al., 2021)	91.83 \pm 0.25	90.15 \pm 0.33	67.15 \pm 0.21	56.48 \pm 0.19	91.03 \pm 0.12	86.15 \pm 0.25	51.13 \pm 0.30	37.86 \pm 0.19
W-MSE (Ermolov et al., 2021)	91.99 \pm 0.12	89.87 \pm 0.25	67.64 \pm 0.16	56.45 \pm 0.26	91.75 \pm 0.23	88.59 \pm 0.15	49.22 \pm 0.16	35.44 \pm 0.10
RELIC v2 (Tomasev et al., 2022)	91.92 \pm 0.14	90.02 \pm 0.22	67.66 \pm 0.20	57.03 \pm 0.18	91.10 \pm 0.23	88.66 \pm 0.12	49.33 \pm 0.13	35.52 \pm 0.22
LMCL (Chen et al., 2021)	91.91 \pm 0.25	88.52 \pm 0.29	67.01 \pm 0.18	56.86 \pm 0.14	90.87 \pm 0.18	85.91 \pm 0.25	49.24 \pm 0.18	32.88 \pm 0.13
ReSSL (Zheng et al., 2021)	90.20 \pm 0.16	88.26 \pm 0.18	66.79 \pm 0.12	53.72 \pm 0.28	88.25 \pm 0.14	86.33 \pm 0.17	46.60 \pm 0.18	32.39 \pm 0.20
SSL-HSIC (Li et al., 2021b)	91.95 \pm 0.14	89.99 \pm 0.17	67.23 \pm 0.26	57.01 \pm 0.27	92.09 \pm 0.20	88.91 \pm 0.29	51.37 \pm 0.15	36.03 \pm 0.12
CorInfoMax (Ozsoy et al., 2022)	91.81 \pm 0.11	89.85 \pm 0.13	67.09 \pm 0.24	56.92 \pm 0.23	91.85 \pm 0.25	89.99 \pm 0.24	51.23 \pm 0.14	35.98 \pm 0.09
MEC (Liu et al., 2022a)	90.55 \pm 0.22	87.80 \pm 0.10	67.36 \pm 0.27	57.25 \pm 0.25	91.33 \pm 0.14	89.03 \pm 0.33	50.93 \pm 0.13	36.28 \pm 0.14
VICRegL (Bardes et al., 2022)	90.99 \pm 0.13	88.75 \pm 0.26	68.03 \pm 0.32	57.34 \pm 0.29	92.12 \pm 0.26	90.01 \pm 0.20	51.52 \pm 0.13	36.24 \pm 0.16
SimCLR + GeSSL	93.15 \pm 0.25	91.02 \pm 0.16	69.23 \pm 0.20	58.56 \pm 0.18	93.15 \pm 0.28	91.55 \pm 0.17	53.54 \pm 0.21	37.16 \pm 0.27
MoCo + GeSSL	92.78 \pm 0.19	89.15 \pm 0.22	68.16 \pm 0.14	59.22 \pm 0.24	93.17 \pm 0.18	88.96 \pm 0.30	52.07 \pm 0.15	37.22 \pm 0.13
BYOL + GeSSL	93.85 \pm 0.22	92.44 \pm 0.30	69.15 \pm 0.22	58.99 \pm 0.16	94.45 \pm 0.18	90.50 \pm 0.17	54.84 \pm 0.19	37.54 \pm 0.26
Barlow Twins + GeSSL	92.99 \pm 0.18	91.02 \pm 0.17	69.56 \pm 0.19	59.93 \pm 0.17	93.84 \pm 0.09	89.46 \pm 0.25	52.65 \pm 0.14	35.15 \pm 0.16
SwAV + GeSSL	93.17 \pm 0.20	89.98 \pm 0.26	69.98 \pm 0.24	59.36 \pm 0.25	92.85 \pm 0.29	91.68 \pm 0.24	51.89 \pm 0.24	36.78 \pm 0.34
DINO + GeSSL	92.77 \pm 0.23	92.12 \pm 0.23	70.85 \pm 0.18	61.68 \pm 0.33	94.48 \pm 0.29	91.48 \pm 0.19	53.51 \pm 0.26	37.89 \pm 0.24

Table 2. The Top-1 and Top-5 classification accuracies of linear classifier on the ImageNet-100 dataset and ImageNet dataset (200 Epochs) with ResNet-50 as feature extractor.

Method	ImageNet-100		ImageNet	
	Top-1	Top-5	Top-1	Top-5
SimCLR (Chen et al., 2020a)	70.15 \pm 0.16	89.75 \pm 0.14	68.32 \pm 0.31	89.76 \pm 0.23
MoCo (Chen et al., 2020b)	72.80 \pm 0.12	91.64 \pm 0.11	67.55 \pm 0.27	88.42 \pm 0.11
SimSiam (Chen & He, 2021)	73.01 \pm 0.21	92.61 \pm 0.27	70.02 \pm 0.14	88.76 \pm 0.23
Barlow Twins (Zbontar et al., 2021)	75.97 \pm 0.23	92.91 \pm 0.19	69.94 \pm 0.32	88.97 \pm 0.27
SwAV (Caron et al., 2020)	75.78 \pm 0.16	92.86 \pm 0.15	69.12 \pm 0.24	89.38 \pm 0.20
DINO (Caron et al., 2021)	75.43 \pm 0.18	93.32 \pm 0.19	70.58 \pm 0.24	91.32 \pm 0.27
W-MSE (Ermolov et al., 2021)	76.01 \pm 0.27	93.12 \pm 0.21	70.85 \pm 0.31	91.57 \pm 0.20
RELIC v2 (Tomasev et al., 2022)	75.88 \pm 0.15	93.52 \pm 0.13	70.98 \pm 0.21	91.15 \pm 0.26
LMCL (Chen et al., 2021)	75.89 \pm 0.19	92.89 \pm 0.28	70.83 \pm 0.26	90.04 \pm 0.21
ReSSL (Zheng et al., 2021)	75.77 \pm 0.21	92.91 \pm 0.27	69.92 \pm 0.24	91.25 \pm 0.12
CorInfoMax (Ozsoy et al., 2022)	75.54 \pm 0.20	92.23 \pm 0.25	70.83 \pm 0.15	91.53 \pm 0.22
MEC (Liu et al., 2022a)	75.38 \pm 0.17	92.84 \pm 0.20	70.34 \pm 0.27	91.25 \pm 0.38
VICRegL (Bardes et al., 2022)	75.96 \pm 0.19	92.97 \pm 0.26	70.24 \pm 0.27	91.60 \pm 0.24
SimCLR + GeSSL	72.43 \pm 0.18	91.87 \pm 0.21	69.65 \pm 0.16	90.98 \pm 0.19
MoCo + GeSSL	73.78 \pm 0.19	93.28 \pm 0.23	69.47 \pm 0.28	90.34 \pm 0.28
SimSiam + GeSSL	75.48 \pm 0.19	94.83 \pm 0.31	71.74 \pm 0.19	89.28 \pm 0.30
Barlow Twins + GeSSL	76.83 \pm 0.19	93.23 \pm 0.18	71.89 \pm 0.22	89.32 \pm 0.14
SwAV + GeSSL	76.38 \pm 0.20	95.47 \pm 0.19	71.47 \pm 0.10	90.28 \pm 0.28
DINO + GeSSL	76.84 \pm 0.25	94.98 \pm 0.24	72.84 \pm 0.19	93.54 \pm 0.18
VICRegL + GeSSL	77.58 \pm 0.22	95.46 \pm 0.15	73.54 \pm 0.29	93.17 \pm 0.30

1000 epochs, the improvement brought by GeSSL reaches an average of 2.7% on Top-1 and an average of 1.4% on Top-5. When only 10% of the labels are available in 1000 epochs, applying GeSSL yields better top-1 and top-5 accuracy, increasing by 1.3% and 2.0%, respectively.

6.4. Transfer Learning

We construct three sets of transfer learning experiments, including the most commonly used object detection and instance segmentation protocol (Chen et al., 2020a; Zbontar et al., 2021; Grill et al., 2020), transfer to other domains (different datasets), and transfer learning on video-based tasks. Here, we present the first experiment, i.e., the most commonly used protocol for transfer learning, and the other

Table 3. The semi-supervised learning accuracies ($\pm 95\%$ confidence interval) on the ImageNet dataset with the ResNet-50 pre-trained on the Imagenet dataset.

Method	Epochs	1%		10%	
		Top-1	Top-5	Top-1	Top-5
MoCo (Chen et al., 2020b)	200	43.8 \pm 0.2	72.3 \pm 0.1	61.9 \pm 0.1	84.6 \pm 0.2
BYOL (Grill et al., 2020)	200	54.8 \pm 0.2	78.8 \pm 0.1	68.0 \pm 0.2	88.5 \pm 0.2
BYOL + GeSSL	200	46.2 \pm 0.3	74.3 \pm 0.2	63.4 \pm 0.2	85.3 \pm 0.1
MoCo + GeSSL	200	56.9 \pm 0.2	79.6 \pm 0.1	70.8 \pm 0.2	89.9 \pm 0.2
SimCLR (Chen et al., 2020a)	1000	48.3 \pm 0.2	75.5 \pm 0.1	65.6 \pm 0.1	87.8 \pm 0.2
MoCo (Chen et al., 2020b)	1000	52.3 \pm 0.1	77.9 \pm 0.2	68.4 \pm 0.1	88.0 \pm 0.2
BYOL (Grill et al., 2020)	1000	56.3 \pm 0.2	79.6 \pm 0.2	69.7 \pm 0.2	89.3 \pm 0.1
SimSiam (Chen & He, 2021)	1000	54.9 \pm 0.2	79.5 \pm 0.2	68.0 \pm 0.1	89.0 \pm 0.3
Barlow Twins (Zbontar et al., 2021)	1000	55.0 \pm 0.1	79.2 \pm 0.1	67.7 \pm 0.2	89.3 \pm 0.2
RELIC v2 (Tomasev et al., 2022)	1000	55.2 \pm 0.2	80.0 \pm 0.1	68.0 \pm 0.2	88.9 \pm 0.2
LMCL (Chen et al., 2021)	1000	54.8 \pm 0.2	79.4 \pm 0.2	70.3 \pm 0.1	89.9 \pm 0.2
ReSSL (Zheng et al., 2021)	1000	55.0 \pm 0.1	79.6 \pm 0.3	69.9 \pm 0.1	89.7 \pm 0.1
SSL-HSIC (Li et al., 2021b)	1000	55.4 \pm 0.3	80.1 \pm 0.2	70.4 \pm 0.1	90.0 \pm 0.1
CorInfoMax (Ozsoy et al., 2022)	1000	55.0 \pm 0.2	79.6 \pm 0.3	70.3 \pm 0.2	89.3 \pm 0.2
MEC (Liu et al., 2022a)	1000	54.8 \pm 0.1	79.4 \pm 0.2	70.0 \pm 0.1	89.1 \pm 0.1
VICRegL (Bardes et al., 2022)	1000	54.9 \pm 0.1	79.6 \pm 0.2	67.2 \pm 0.1	89.4 \pm 0.2
SimCLR + GeSSL	1000	50.4 \pm 0.2	77.5 \pm 0.1	66.9 \pm 0.2	89.4 \pm 0.3
MoCo + GeSSL	1000	53.5 \pm 0.2	78.7 \pm 0.1	70.9 \pm 0.2	89.0 \pm 0.2
BYOL + GeSSL	1000	58.7 \pm 0.3	81.4 \pm 0.2	71.5 \pm 0.1	90.7 \pm 0.2
Barlow Twins + GeSSL	1000	57.4 \pm 0.2	80.2 \pm 0.1	68.8 \pm 0.2	91.4 \pm 0.2

two sets of experiments are described in Appendix F.2.

Experimental setup. We evaluate GeSSL on Pascal VOC and COCO datasets. Specifically, we use Faster R-CNN (Ren et al., 2015) with a C4-backbone (Wu et al., 2019) for the VOC detection task and use Mask R-CNN (He et al., 2017) with the same C4-backbone and a $1 \times$ schedule for the COCO detection and segmentation tasks. During training, we train the Faster R-CNN model on the VOC 07+12 set (16K images) and reduce the initial learning rate by 10 at 18K and 22K iterations, while training on the VOC 07 set (5K images) with fewer iterations. For the Mask R-CNN, we train it on the COCO 2017 train split and report the results on the val split. More details are shown in Appendix F.2.

Results. Table 4 shows the transfer learning results. The

Table 4. The results of transfer learning on object detection and instance segmentation with C4-backbone as the feature extractor. “AP” is the average precision, “AP_N” represents the average precision when the IoU (Intersection and Union Ratio) threshold is N%.

Method	VOC 07 detection			VOC 07+12 detection			COCO detection			COCO instance segmentation		
	AP ₅₀	AP	AP ₇₅	AP ₅₀	AP	AP ₇₅	AP ₅₀	AP	AP ₇₅	AP ₅₀ ^{mask}	AP ^{mask}	AP ₇₅ ^{mask}
Supervised	74.4	42.4	42.7	81.3	53.5	58.8	58.2	38.2	41.2	54.7	33.3	35.2
SimCLR (Chen et al., 2020a)	75.9	46.8	50.1	81.8	55.5	61.4	57.7	37.9	40.9	54.6	33.3	35.3
MoCo (Chen et al., 2020b)	77.1	46.8	52.5	82.5	57.4	64.0	58.9	39.3	42.5	55.8	34.4	36.5
BYOL (Grill et al., 2020)	77.1	47.0	49.9	81.4	55.3	61.1	57.8	37.9	40.9	54.3	33.2	35.0
SimSiam (Chen & He, 2021)	77.3	48.5	52.5	82.4	57.0	63.7	59.3	39.2	42.1	56.0	34.4	36.7
Barlow Twins (Zbontar et al., 2021)	75.7	47.2	50.3	82.6	56.8	63.4	59.0	39.2	42.5	56.0	34.3	36.5
SwAV (Caron et al., 2020)	75.5	46.5	49.6	82.6	56.1	62.7	58.6	38.4	41.3	55.2	33.8	35.9
MEC (Liu et al., 2022a)	77.4	48.3	52.3	82.8	57.5	64.5	59.8	39.8	43.2	56.3	34.7	36.8
RELIC v2 (Tomasev et al., 2022)	76.9	48.0	52.0	82.1	57.3	63.9	58.4	39.3	42.3	56.0	34.6	36.3
CorInfoMax (Ozsoy et al., 2022)	76.8	47.6	52.2	82.4	57.0	63.4	58.8	39.6	42.5	56.2	34.8	36.5
VICRegL (Bardes et al., 2022)	75.9	47.4	52.3	82.6	56.4	62.9	59.2	39.8	42.1	56.5	35.1	36.8
SimCLR + GeSSL	77.4	49.1	51.2	84.3	57.4	62.9	58.5	39.6	43.1	56.3	35.0	36.1
MoCo + GeSSL	78.5	49.3	53.9	85.2	59.3	65.5	60.7	41.6	44.2	58.2	36.1	38.0
BYOL + GeSSL	78.5	49.4	51.7	83.5	57.9	63.2	59.8	39.1	43.0	55.6	34.6	37.9
SimSiam + GeSSL	79.3	50.0	53.7	84.6	58.9	65.2	61.5	41.7	43.4	57.6	36.5	39.0
SwAV + GeSSL	77.2	48.8	51.0	84.1	57.5	65.0	61.4	39.7	43.3	56.2	36.5	37.4
VICRegL + GeSSL	77.4	49.7	53.2	84.5	58.0	64.7	62.1	41.9	44.6	58.1	36.8	38.4

Table 5. The few-shot learning accuracies ($\pm 95\%$ confidence interval) on miniImageNet, Omniglot, and CIFAR-FS with the C4-backbone. More details of the baselines are illustrated in Appendix E. Full results are provided in Appendix F.

Method	Omniglot			miniImageNet			CIFAR-FS		
	(5,1)	(5,5)	(20,1)	(5,1)	(5,5)	(20,1)	(5,1)	(5,5)	(20,1)
<i>Unsupervised Few-shot Learning</i>									
CACTUs (Hsu et al., 2018)	65.29 \pm 0.21	86.25 \pm 0.19	49.54 \pm 0.21	39.32 \pm 0.28	53.54 \pm 0.27	31.99 \pm 0.29	40.02 \pm 0.23	58.16 \pm 0.22	35.88 \pm 0.25
UMTRA (Khodadadeh et al., 2019)	83.32 \pm 0.37	94.23 \pm 0.35	75.84 \pm 0.34	39.23 \pm 0.34	51.78 \pm 0.32	30.27 \pm 0.34	41.61 \pm 0.40	60.55 \pm 0.38	37.10 \pm 0.39
LASIUM (Khodadadeh et al., 2020)	82.38 \pm 0.36	95.11 \pm 0.36	70.23 \pm 0.36	42.12 \pm 0.38	54.98 \pm 0.37	34.26 \pm 0.35	45.33 \pm 0.32	62.65 \pm 0.33	38.40 \pm 0.33
SVEBM (Kong et al., 2021)	87.07 \pm 0.28	94.13 \pm 0.27	73.33 \pm 0.28	44.74 \pm 0.29	58.38 \pm 0.28	39.71 \pm 0.30	47.24 \pm 0.25	63.10 \pm 0.28	40.10 \pm 0.28
GMVAE (Lee et al., 2021)	90.89 \pm 0.32	96.05 \pm 0.32	81.51 \pm 0.33	42.28 \pm 0.36	56.97 \pm 0.38	39.83 \pm 0.36	47.45 \pm 0.36	63.20 \pm 0.35	41.55 \pm 0.35
PsCo (Jang et al., 2023)	96.18 \pm 0.21	98.22 \pm 0.23	89.32 \pm 0.23	46.35 \pm 0.24	63.05 \pm 0.23	40.84 \pm 0.27	51.77 \pm 0.27	69.66 \pm 0.26	45.08 \pm 0.27
<i>Self-supervised Learning</i>									
SimCLR (Chen et al., 2020a)	90.83 \pm 0.21	97.67 \pm 0.21	81.67 \pm 0.23	42.32 \pm 0.38	51.10 \pm 0.37	36.36 \pm 0.36	49.44 \pm 0.30	60.02 \pm 0.29	39.29 \pm 0.30
MoCo (Chen et al., 2020b)	87.83 \pm 0.20	95.52 \pm 0.19	80.03 \pm 0.21	40.56 \pm 0.34	49.41 \pm 0.37	36.52 \pm 0.38	45.35 \pm 0.31	58.11 \pm 0.32	37.89 \pm 0.32
SwAV (Caron et al., 2020)	91.28 \pm 0.19	97.21 \pm 0.20	82.02 \pm 0.20	44.39 \pm 0.36	54.91 \pm 0.36	37.13 \pm 0.37	49.39 \pm 0.29	62.20 \pm 0.30	40.19 \pm 0.32
SimCLR + GeSSL	94.15 \pm 0.26	98.46 \pm 0.15	90.15 \pm 0.19	46.34 \pm 0.25	62.18 \pm 0.20	39.28 \pm 0.19	52.18 \pm 0.32	67.01 \pm 0.19	46.23 \pm 0.27
MoCo + GeSSL	92.78 \pm 0.24	97.26 \pm 0.23	88.01 \pm 0.24	46.66 \pm 0.25	60.48 \pm 0.25	40.38 \pm 0.19	50.98 \pm 0.24	65.56 \pm 0.11	44.23 \pm 0.17
SwAV + GeSSL	95.48 \pm 0.16	97.98 \pm 0.20	91.17 \pm 0.25	48.15 \pm 0.18	63.28 \pm 0.09	41.32 \pm 0.28	51.98 \pm 0.31	69.28 \pm 0.29	47.28 \pm 0.18

Table 6. Ablation study of hyperparameter λ for self-motivated target with different K on miniImageNet.

K	λ				K \times λ								Acc (%)	Training hours	
	1	5	10	15	2	6	10	11	15	16	20	25			30
✓	✓				✓									41.1 \pm 0.3	3.15
✓		✓				✓								44.3 \pm 0.4	3.28
✓			✓				✓							46.5 \pm 0.3	3.40
✓				✓				✓						45.7 \pm 0.3	3.51
	✓					✓								45.4 \pm 0.2	3.69
		✓					✓							47.0 \pm 0.3	3.80
			✓					✓						46.9 \pm 0.3	4.01
				✓					✓					47.1 \pm 0.3	4.27
					✓					✓				46.8 \pm 0.4	4.52
						✓					✓			47.2 \pm 0.3	5.07

results show the great performance improvements achieved by GeSSL: (i) for the VOC 07 detection task, SimSiam + GeSSL and MoCo + GeSSL achieve the best performance; (ii) for the VOC 07+12 detection task, MoCo + GeSSL outperforms other methods; (iii) for the COCO detection task, GeSSL applied to VICRegL obtains the best results; and (iv) for the COCO instance segmentation task, MoCo + GeSSL and VICRegL + GeSSL obtain the best results. Therefore,

our GeSSL continues to exhibit remarkable performance.

6.5. Few-shot Learning

Experimental setup. We adopt the commonly used protocol for few-shot learning (Jang et al., 2023). We evaluate our GeSSL on three few-shot benchmarks, i.e., miniImageNet, Omniglot, and CIFAR-FS. For few-shot SSL task construction, we first randomly select N samples without class-level overlap for each task, and then apply K -times data augmentation, obtaining a N -way K -shot task with N classes and $N \times K$ samples. We use the stochastic gradient descent (SGD) optimizer, setting the momentum and weight decay values to 0.9 and 10^{-4} respectively. We evaluate the trained model’s performance in a new class, where we randomly take some unseen samples to calculate the accuracy.

Results. Table 5 shows the standard few-shot learning results of GeSSL compared with the baselines. From the re-

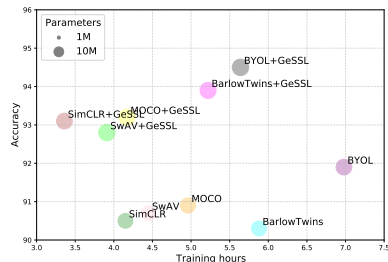


Figure 2. Model efficiency comparison, which is recorded with the same batch size and official code configuration.

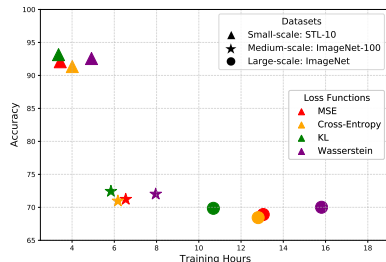


Figure 3. Ablation study of loss functions. The settings of the comparison losses will be provided in Appendix G.3.

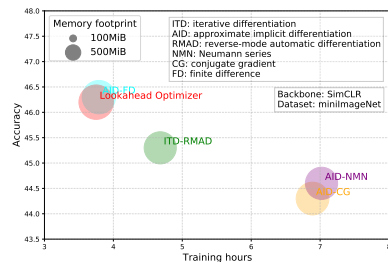


Figure 4. Implementation of the bi-level optimization. All differentiation methods are described in detail in Appendix G.4.

sults, we can see that our framework still achieve remarkable performance improvement, demonstrating the outstanding robustness and superiority of GeSSL. Specifically, we can observe that: (i) applying GeSSL outperforms the SOTA few-shot learning baselines on almost all the datasets; and (ii) applying GeSSL to the SSL models result in significant performance improvement (an average of nearly 8%) across all tasks. We also conducted experiments on the cross-domain few-shot learning scenario, and the results still proved the outstanding effect of our method. More details and results are illustrated in Appendix F.3.

6.6. Ablation Study and Analysis

Model efficiency; (iii) Role of loss; (iv) Implementation of bi-level optimization. In this section, we conduct ablation studies and analysis for four aspects: (i) Influence of λ , (ii) Model efficiency, (iii) Role of loss, and (iv) Implementation of the bi-level optimization. All the experiments are apples-to-apples comparisons, more details are provided in Appendix G.

Influence of λ . We evaluate the performance (accuracy(%) and training hours) of SimCLR + GeSSL with different λ under different K (the number of update steps in the first-level optimization), following the same implementation discussed in Subsection 6.5. The results in Table 6 show that the performance is optimal when $\lambda = 10$ under $K = 1$ or $K = 5$. If λ or K continues to increase, the performance improvement will be negligible but with higher time costs.

Model efficiency. Next, we compare the trade-off performance of multiple baselines before and after using our GeSSL on STL-10 (Coates et al., 2011) with ResNet-50 backbone. The results illustrated in Figure 2 show that our GeSSL achieves great performance and computational efficiency improvements with acceptable parameter size. Appendix G.4 provides all numerical results of this comparison experiment, including memory footprint, parameter size, training time, and performance (accuracy). The results show that although GeSSL brings larger memory footprint and parameter size costs, it is relatively negligible compared to the great performance and efficiency improvements.

Role of loss. We also evaluate the impact of the loss function in the second-level optimization. We record the performance and training time of SimCLR + GeSSL with different losses, including MSE, Cross-Entropy, KL divergence, and Wasserstein distance. As shown in Figure 3, the self-motivated target with KL divergence achieves the best trade-off between accuracy and computational efficiency, i.e., achieves excellent results in a short training time.

Implementation of the bi-level optimization. The gradient update requires composing best-response Jacobians via the chain rule, and the way of differentiation directly affects the model efficiency. Therefore, we analyze the accuracy, training time, and memory footprint of different differentiation methods following (Choe et al., 2022; Liu et al., 2018; Zhang et al., 2019). The results of Figure 4 show that approximate implicit differentiation with finite difference (AID-FD) achieves the optimal results, and our optimization process is also conducted following this setting.

7. Conclusion

In this study, we explore the generality of self-supervised learning (SSL). We provide a theoretical understanding and mathematical expression of the generality in SSL, and define a σ -measurement to quantify it. Based on this insight, we further propose a novel SSL framework (GeSSL) to explicitly model generality into the learning objective through bi-level optimization. It introduces a σ -measurement-based self-motivated target to guide the model to learn along the best update direction. We provide rigorous theoretical support for performance guarantees. Extensive experiments on various benchmark datasets and downstream tasks demonstrate the superior robustness and generalization of GeSSL. We hope that this work can bring us one step closer to general machine learning for real-world applications.

Limitations Desipe GeSSL is generally effective for essentially all cases it has been tried, its limitations may come from the fact that GeSSL brings larger parameter size and memory footprint costs. However, this is relatively negligible compared to the great performance and computational

efficiency improvement brought by GeSSL.

Impact Statements

This work aims to advance the field of Machine Learning. The proposed method opens up interesting future research directions and provides a powerful idea for generality. There are many potential societal consequences of our work, none of which we feel must be specifically highlighted here.

References

- Aberdam, A., Litman, R., Tsiper, S., Anshel, O., Slossberg, R., Mazor, S., Manmatha, R., and Perona, P. Sequence-to-sequence contrastive learning for text recognition. In *Proceedings of the IEEE/CVF Conference on Computer Vision and Pattern Recognition*, pp. 15302–15312, 2021.
- Araslanov, N. and Roth, S. Self-supervised augmentation consistency for adapting semantic segmentation. In *Proceedings of the IEEE/CVF Conference on Computer Vision and Pattern Recognition*, pp. 15384–15394, 2021.
- Atito, S., Awais, M., and Kittler, J. Sit: Self-supervised vision transformer. *arXiv preprint arXiv:2104.03602*, 2021.
- Baevski, A., Hsu, W.-N., Xu, Q., Babu, A., Gu, J., and Auli, M. Data2vec: A general framework for self-supervised learning in speech, vision and language. In *International Conference on Machine Learning*, pp. 1298–1312. PMLR, 2022.
- Baevski, A., Babu, A., Hsu, W.-N., and Auli, M. Efficient self-supervised learning with contextualized target representations for vision, speech and language. In *International Conference on Machine Learning*, pp. 1416–1429. PMLR, 2023.
- Balazevic, I., Steiner, D., Parthasarathy, N., Arandjelović, R., and Henaff, O. Towards in-context scene understanding. *Advances in Neural Information Processing Systems*, 36, 2024.
- Bansal, Y., Kaplun, G., and Barak, B. For self-supervised learning, rationality implies generalization, provably. *arXiv preprint arXiv:2010.08508*, 2020.
- Bardes, A., Ponce, J., and LeCun, Y. Vicregl: Self-supervised learning of local visual features. *arXiv preprint arXiv:2210.01571*, 2022.
- Bertinetto, L., Henriques, J. F., Torr, P. H., and Vedaldi, A. Meta-learning with differentiable closed-form solvers. *arXiv preprint arXiv:1805.08136*, 2018.
- Bossard, L., Guillaumin, M., and Van Gool, L. Food-101—mining discriminative components with random forests. In *Computer Vision—ECCV 2014: 13th European Conference, Zurich, Switzerland, September 6–12, 2014, Proceedings, Part VI 13*, pp. 446–461. Springer, 2014.
- Botev, Z. I., Kroese, D. P., Rubinstein, R. Y., and L’Ecuyer, P. The cross-entropy method for optimization. In *Handbook of statistics*, volume 31, pp. 35–59. Elsevier, 2013.
- Caron, M., Bojanowski, P., Joulin, A., and Douze, M. Deep clustering for unsupervised learning of visual features. In *Proceedings of the European conference on computer vision (ECCV)*, pp. 132–149, 2018.
- Caron, M., Misra, I., Mairal, J., Goyal, P., Bojanowski, P., and Joulin, A. Unsupervised learning of visual features by contrasting cluster assignments. *Advances in neural information processing systems*, 33:9912–9924, 2020.
- Caron, M., Touvron, H., Misra, I., Jégou, H., Mairal, J., Bojanowski, P., and Joulin, A. Emerging properties in self-supervised vision transformers. In *Proceedings of the IEEE/CVF international conference on computer vision*, pp. 9650–9660, 2021.
- Chen, S., Niu, G., Gong, C., Li, J., Yang, J., and Sugiyama, M. Large-margin contrastive learning with distance polarization regularizer. In *International Conference on Machine Learning*, pp. 1673–1683. PMLR, 2021.
- Chen, T., Kornblith, S., Norouzi, M., and Hinton, G. A simple framework for contrastive learning of visual representations. In *International conference on machine learning*, pp. 1597–1607. PMLR, 2020a.
- Chen, X. and He, K. Exploring simple siamese representation learning. In *Proceedings of the IEEE/CVF conference on computer vision and pattern recognition*, pp. 15750–15758, 2021.
- Chen, X., Fan, H., Girshick, R., and He, K. Improved baselines with momentum contrastive learning. *arXiv preprint arXiv:2003.04297*, 2020b.
- Chicco, D., Warrens, M. J., and Jurman, G. The coefficient of determination r-squared is more informative than smape, mape, mape, mse and rmse in regression analysis evaluation. *PeerJ Computer Science*, 7:e623, 2021.
- Choe, S. K., Neiswanger, W., Xie, P., and Xing, E. Betty: An automatic differentiation library for multilevel optimization. *arXiv preprint arXiv:2207.02849*, 2022.
- Coates, A., Ng, A., and Lee, H. An Analysis of Single-Layer Networks in Unsupervised Feature Learning. In *Proceedings of the Fourteenth International Conference on Artificial Intelligence and Statistics*, pp. 215–223. JMLR Workshop and Conference Proceedings, June 2011.

- Codella, N. C., Gutman, D., Celebi, M. E., Helba, B., Marchetti, M. A., Dusza, S. W., Kalloo, A., Liopyris, K., Mishra, N., Kittler, H., et al. Skin lesion analysis toward melanoma detection: A challenge at the 2017 international symposium on biomedical imaging (isbi), hosted by the international skin imaging collaboration (isic). In *2018 IEEE 15th international symposium on biomedical imaging (ISBI 2018)*, pp. 168–172. IEEE, 2018.
- De Boer, P.-T., Kroese, D. P., Mannor, S., and Rubinstein, R. Y. A tutorial on the cross-entropy method. *Annals of operations research*, 134:19–67, 2005.
- Deng, J., Dong, W., Socher, R., Li, L.-J., Li, K., and Fei-Fei, L. ImageNet: A large-scale hierarchical image database. In *2009 IEEE Conference on Computer Vision and Pattern Recognition*, pp. 248–255, June 2009. doi: 10.1109/CVPR.2009.5206848.
- Dosovitskiy, A., Beyer, L., Kolesnikov, A., Weissenborn, D., Zhai, X., Unterthiner, T., Dehghani, M., Minderer, M., Heigold, G., Gelly, S., et al. An image is worth 16x16 words: Transformers for image recognition at scale. *arXiv preprint arXiv:2010.11929*, 2020.
- Eastwood, C., von Kügelgen, J., Ericsson, L., Bouchacourt, D., Vincent, P., Schölkopf, B., and Ibrahim, M. Self-supervised disentanglement by leveraging structure in data augmentations. *arXiv preprint arXiv:2311.08815*, 2023.
- Ericsson, L., Gouk, H., Loy, C. C., and Hospedales, T. M. Self-supervised representation learning: Introduction, advances, and challenges. *IEEE Signal Processing Magazine*, 39(3):42–62, 2022.
- Ermolov, A., Siarohin, A., Sangineto, E., and Sebe, N. Whitening for self-supervised representation learning. In *International Conference on Machine Learning*, pp. 3015–3024. PMLR, 2021.
- Everingham, M., Van Gool, L., Williams, C. K., Winn, J., and Zisserman, A. The pascal visual object classes (voc) challenge. *International journal of computer vision*, 88(2):303–338, 2010.
- Finn, C., Abbeel, P., and Levine, S. Model-agnostic meta-learning for fast adaptation of deep networks. In *International conference on machine learning*, pp. 1126–1135. PMLR, 2017.
- Goldberger, Gordon, and Greenspan. An efficient image similarity measure based on approximations of kl-divergence between two gaussian mixtures. In *Proceedings Ninth IEEE International conference on computer vision*, pp. 487–493. IEEE, 2003.
- Gong, C., Wang, D., and Liu, Q. Alphamatch: Improving consistency for semi-supervised learning with alpha-divergence. In *Proceedings of the IEEE/CVF conference on computer vision and pattern recognition*, pp. 13683–13692, 2021.
- Goyal, P., Caron, M., Lefaudeaux, B., Xu, M., Wang, P., Pai, V., Singh, M., Liptchinsky, V., Misra, I., Joulin, A., et al. Self-supervised pretraining of visual features in the wild. *arXiv preprint arXiv:2103.01988*, 2021.
- Grazzi, R., Franceschi, L., Pontil, M., and Salzo, S. On the iteration complexity of hypergradient computation. In *International Conference on Machine Learning*, pp. 3748–3758. PMLR, 2020.
- Grill, J.-B., Strub, F., Altché, F., Tallec, C., Richemond, P., Buchatskaya, E., Doersch, C., Avila Pires, B., Guo, Z., Gheshlaghi Azar, M., et al. Bootstrap your own latent—a new approach to self-supervised learning. *Advances in neural information processing systems*, 33:21271–21284, 2020.
- Guo, Y., Codella, N. C., Karlinsky, L., Codella, J. V., Smith, J. R., Saenko, K., Rosing, T., and Feris, R. A broader study of cross-domain few-shot learning. In *Computer Vision—ECCV 2020: 16th European Conference, Glasgow, UK, August 23–28, 2020, Proceedings, Part XXVII 16*, pp. 124–141. Springer, 2020.
- He, K., Gkioxari, G., Dollár, P., and Girshick, R. Mask r-cnn. In *Proceedings of the IEEE international conference on computer vision*, pp. 2961–2969, 2017.
- Hershey, J. R. and Olsen, P. A. Approximating the kullback-leibler divergence between gaussian mixture models. In *2007 IEEE International Conference on Acoustics, Speech and Signal Processing-ICASSP’07*, volume 4, pp. IV–317. IEEE, 2007.
- Hodosh, M., Young, P., and Hockenmaier, J. Framing image description as a ranking task: Data, models and evaluation metrics. *Journal of Artificial Intelligence Research*, 47: 853–899, 2013.
- Hou, Z., Liu, X., Cen, Y., Dong, Y., Yang, H., Wang, C., and Tang, J. Graphmae: Self-supervised masked graph autoencoders. In *Proceedings of the 28th ACM SIGKDD Conference on Knowledge Discovery and Data Mining*, pp. 594–604, 2022.
- Hsu, K., Levine, S., and Finn, C. Unsupervised learning via meta-learning. *arXiv preprint arXiv:1810.02334*, 2018.
- Huang, W., Yi, M., and Zhao, X. Towards the generalization of contrastive self-supervised learning. *arXiv preprint arXiv:2111.00743*, 2021.

- Jaiswal, A., Babu, A. R., Zadeh, M. Z., Banerjee, D., and Makedon, F. A survey on contrastive self-supervised learning. *Technologies*, 9(1):2, 2020.
- Jang, H., Lee, H., and Shin, J. Unsupervised meta-learning via few-shot pseudo-supervised contrastive learning. *arXiv preprint arXiv:2303.00996*, 2023.
- Joshi, S. and Mirzasoleiman, B. Data-efficient contrastive self-supervised learning: Most beneficial examples for supervised learning contribute the least. In *International conference on machine learning*, pp. 15356–15370. PMLR, 2023.
- Kang, M., Song, H., Park, S., Yoo, D., and Pereira, S. Benchmarking self-supervised learning on diverse pathology datasets. In *Proceedings of the IEEE/CVF Conference on Computer Vision and Pattern Recognition*, pp. 3344–3354, 2023.
- Khodadadeh, S., Boloni, L., and Shah, M. Unsupervised meta-learning for few-shot image classification. *Advances in neural information processing systems*, 32, 2019.
- Khodadadeh, S., Zehtabian, S., Vahidian, S., Wang, W., Lin, B., and Bölöni, L. Unsupervised meta-learning through latent-space interpolation in generative models. *arXiv preprint arXiv:2006.10236*, 2020.
- Kong, D., Pang, B., and Wu, Y. N. Unsupervised meta-learning via latent space energy-based model of symbol vector coupling. In *Fifth Workshop on Meta-Learning at the Conference on Neural Information Processing Systems*, 2021.
- Krause, J., Stark, M., Deng, J., and Fei-Fei, L. 3d object representations for fine-grained categorization. In *Proceedings of the IEEE international conference on computer vision workshops*, pp. 554–561, 2013.
- Krishnan, R., Rajpurkar, P., and Topol, E. J. Self-supervised learning in medicine and healthcare. *Nature Biomedical Engineering*, 6(12):1346–1352, 2022.
- Krizhevsky, A., Hinton, G., et al. Learning multiple layers of features from tiny images. 2009.
- Lake, B. M., Salakhutdinov, R., and Tenenbaum, J. B. The omniglot challenge: a 3-year progress report. *Current Opinion in Behavioral Sciences*, 29:97–104, 2019.
- Le, Y. and Yang, X. Tiny imagenet visual recognition challenge. *CS 231N*, 7(7):3, 2015.
- Lebanon, G. Bias, variance, and mse of estimators. *Georgia Institute of Technology. Atlanta*, 2010.
- Lee, D. B., Min, D., Lee, S., and Hwang, S. J. Meta-gmvae: Mixture of gaussian vae for unsupervised meta-learning. In *International Conference on Learning Representations*, 2021.
- Li, C., Yang, J., Zhang, P., Gao, M., Xiao, B., Dai, X., Yuan, L., and Gao, J. Efficient self-supervised vision transformers for representation learning. *arXiv preprint arXiv:2106.09785*, 2021a.
- Li, D., Yang, Y., Song, Y.-Z., and Hospedales, T. M. Deeper, broader and artier domain generalization. In *Proceedings of the IEEE international conference on computer vision*, pp. 5542–5550, 2017.
- Li, X., Liu, S., Kim, K., De Mello, S., Jampani, V., Yang, M.-H., and Kautz, J. Self-supervised single-view 3d reconstruction via semantic consistency. In *Computer Vision—ECCV 2020: 16th European Conference, Glasgow, UK, August 23–28, 2020, Proceedings, Part XIV 16*, pp. 677–693. Springer, 2020.
- Li, Y., Pogodin, R., Sutherland, D. J., and Gretton, A. Self-supervised learning with kernel dependence maximization. *Advances in Neural Information Processing Systems*, 34:15543–15556, 2021b.
- Lin, T.-Y., Maire, M., Belongie, S., Hays, J., Perona, P., Ramanan, D., Dollár, P., and Zitnick, C. L. Microsoft coco: Common objects in context. In *European conference on computer vision*, pp. 740–755. Springer, 2014.
- Liu, H., Simonyan, K., and Yang, Y. Darts: Differentiable architecture search. *arXiv preprint arXiv:1806.09055*, 2018.
- Liu, X., Wang, Z., Li, Y.-L., and Wang, S. Self-supervised learning via maximum entropy coding. *Advances in Neural Information Processing Systems*, 35:34091–34105, 2022a.
- Liu, X., Wang, Z., Li, Y.-L., and Wang, S. Self-supervised learning via maximum entropy coding. *Advances in Neural Information Processing Systems*, 35:34091–34105, 2022b.
- Lorraine, J., Vicol, P., and Duvenaud, D. Optimizing millions of hyperparameters by implicit differentiation. In *International conference on artificial intelligence and statistics*, pp. 1540–1552. PMLR, 2020.
- Maji, S., Rahtu, E., Kannala, J., Blaschko, M., and Vedaldi, A. Fine-grained visual classification of aircraft. *arXiv preprint arXiv:1306.5151*, 2013.
- Marmolin, H. Subjective mse measures. *IEEE transactions on systems, man, and cybernetics*, 16(3):486–489, 1986.

- McCarthy, J. Generality in artificial intelligence. *Communications of the ACM*, 30(12):1030–1035, 1987.
- Milan, A., Leal-Taixé, L., Reid, I., Roth, S., and Schindler, K. Mot16: A benchmark for multi-object tracking. *arXiv preprint arXiv:1603.00831*, 2016.
- Mohamed, A., Demidov, D., and Sebaitre, Z. Image captioning through self-supervised learning. Technical report, Technical Report, 2022.
- Mohanty, S. P., Hughes, D. P., and Salathé, M. Using deep learning for image-based plant disease detection. *Frontiers in plant science*, 7:1419, 2016.
- Mohri, M., Rostamizadeh, A., and Talwalkar, A. *Foundations of machine learning*. MIT press, 2018.
- Ni, R., Shu, M., Souri, H., Goldblum, M., and Goldstein, T. The close relationship between contrastive learning and meta-learning. In *International Conference on Learning Representations*, 2021.
- Nilsback, M.-E. and Zisserman, A. Automated flower classification over a large number of classes. In *2008 Sixth Indian conference on computer vision, graphics & image processing*, pp. 722–729. IEEE, 2008.
- Ozsoy, S., Hamdan, S., Arik, S., Yuret, D., and Erdogan, A. Self-supervised learning with an information maximization criterion. *Advances in Neural Information Processing Systems*, 35:35240–35253, 2022.
- Panaretos, V. M. and Zemel, Y. Statistical aspects of wasserstein distances. *Annual review of statistics and its application*, 6:405–431, 2019.
- Perazzi, F., Pont-Tuset, J., McWilliams, B., Van Gool, L., Gross, M., and Sorkine-Hornung, A. A benchmark dataset and evaluation methodology for video object segmentation. In *Proceedings of the IEEE conference on computer vision and pattern recognition*, pp. 724–732, 2016.
- Rajeswaran, A., Finn, C., Kakade, S. M., and Levine, S. Meta-learning with implicit gradients. *Advances in neural information processing systems*, 32, 2019.
- Ren, S., He, K., Girshick, R., and Sun, J. Faster r-cnn: Towards real-time object detection with region proposal networks. *Advances in neural information processing systems*, 28, 2015.
- Risi, S. and Togelius, J. Increasing generality in machine learning through procedural content generation. *Nature Machine Intelligence*, 2(8):428–436, 2020.
- Schiappa, M. C., Rawat, Y. S., and Shah, M. Self-supervised learning for videos: A survey. *ACM Computing Surveys*, 2022.
- Shahrampour, S., Beirami, A., and Tarokh, V. On data-dependent random features for improved generalization in supervised learning. In *Proceedings of the AAAI Conference on Artificial Intelligence*, volume 32, 2018.
- Shen, Z., Liu, J., He, Y., Zhang, X., Xu, R., Yu, H., and Cui, P. Towards out-of-distribution generalization: A survey. *arXiv preprint arXiv:2108.13624*, 2021.
- Shlens, J. Notes on kullback-leibler divergence and likelihood. *arXiv preprint arXiv:1404.2000*, 2014.
- Shurrah, S. and Duwairi, R. Self-supervised learning methods and applications in medical imaging analysis: A survey. *PeerJ Computer Science*, 8:e1045, 2022.
- Sun, X., Panda, R., Feris, R., and Saenko, K. Adashare: Learning what to share for efficient deep multi-task learning. *Advances in Neural Information Processing Systems*, 33:8728–8740, 2020.
- Tang, J., Wu, S., Sun, J., and Su, H. Cross-domain collaboration recommendation. In *Proceedings of the 18th ACM SIGKDD international conference on Knowledge discovery and data mining*, pp. 1285–1293, 2012.
- Tendle, A. and Hasan, M. R. A study of the generalizability of self-supervised representations. *Machine Learning with Applications*, 6:100124, 2021.
- Tian, Y., Krishnan, D., and Isola, P. Contrastive Multiview Coding, December 2020.
- Tomasev, N., Bica, I., McWilliams, B., Buesing, L., Pascanu, R., Blundell, C., and Mitrovic, J. Pushing the limits of self-supervised resnets: Can we outperform supervised learning without labels on imagenet? *arXiv preprint arXiv:2201.05119*, 2022.
- Tsai, Y.-H. H., Wu, Y., Salakhutdinov, R., and Morency, L.-P. Self-supervised learning from a multi-view perspective. *arXiv preprint arXiv:2006.05576*, 2020.
- Vallender, S. Calculation of the wasserstein distance between probability distributions on the line. *Theory of Probability & Its Applications*, 18(4):784–786, 1974.
- Vinyals, O., Blundell, C., Lillicrap, T., Wierstra, D., et al. Matching networks for one shot learning. *Advances in neural information processing systems*, 29, 2016a.
- Vinyals, O., Toshev, A., Bengio, S., and Erhan, D. Show and tell: Lessons learned from the 2015 mscoco image captioning challenge. *IEEE transactions on pattern analysis and machine intelligence*, 39(4):652–663, 2016b.

- Wang, X., Peng, Y., Lu, L., Lu, Z., Bagheri, M., and Summers, R. M. Chestx-ray8: Hospital-scale chest x-ray database and benchmarks on weakly-supervised classification and localization of common thorax diseases. In *Proceedings of the IEEE conference on computer vision and pattern recognition*, pp. 2097–2106, 2017.
- Wang, Z., Zhao, H., Li, Y.-L., Wang, S., Torr, P., and Bertinetto, L. Do different tracking tasks require different appearance models? *Advances in Neural Information Processing Systems*, 34:726–738, 2021.
- Welinder, P., Branson, S., Mita, T., Wah, C., Schroff, F., Belongie, S., and Perona, P. Caltech-ucsd birds 200. 2010.
- Wu, Y., Kirillov, A., Massa, F., Lo, W.-Y., and Girshick, R. Detectron2. <https://github.com/facebookresearch/detectron2>, 2019.
- Yasmeen, U., Shah, J. H., Khan, M. A., Ansari, G. J., Rehman, S. U., Sharif, M., Kadry, S., and Nam, Y. Text detection and classification from low quality natural images. *Intell. Autom. Soft Comput.*, 26(4):1251–1266, 2020.
- Zbontar, J., Jing, L., Misra, I., LeCun, Y., and Deny, S. Barlow twins: Self-supervised learning via redundancy reduction. In *International Conference on Machine Learning*, pp. 12310–12320. PMLR, 2021.
- Zhang, M., Lucas, J., Ba, J., and Hinton, G. E. Lookahead optimizer: k steps forward, 1 step back. *Advances in neural information processing systems*, 32, 2019.
- Zheng, M., You, S., Wang, F., Qian, C., Zhang, C., Wang, X., and Xu, C. Rssl: Relational self-supervised learning with weak augmentation. *Advances in Neural Information Processing Systems*, 34:2543–2555, 2021.
- Zheng, Y. Methodologies for cross-domain data fusion: An overview. *IEEE transactions on big data*, 1(1):16–34, 2015.
- Zhou, B., Lapedriza, A., Khosla, A., Oliva, A., and Torralba, A. Places: A 10 million image database for scene recognition. *IEEE transactions on pattern analysis and machine intelligence*, 40(6):1452–1464, 2017.

Appendix

The appendix provides supplementary material and additional details to support the main findings and methods proposed in this paper. It is organized into several sections: Appendix A encompasses the pseudo-code of our GeSSL’s learning process, while Appendix B contains the proofs of the presented theorems. Then, Appendix C presents the implementation and architecture of our GeSSL, aiding in the faithful reproduction of our work. Next, Appendices D and E provide details for all datasets and baselines mentioned in the main text. Furthermore, Appendices F and G showcase additional experiments, full results, and experimental details of the comparison experiments and ablation studies that were omitted in the main paper due to page limitations.

Algorithm 1 Pseudo-Code of the proposed GeSSL

Input: Candidate pool \mathcal{D} ; Randomly initialize SSL model f_θ with a feature extractor $g(\cdot)$, a projection head $h(\cdot)$, and a classification head $c(\cdot)$

Parameter: Mini-batch B ; The number of update steps K in the first-level optimization; The hyperparameter λ in the self-motivated target; Learning rates α and β

Output: The SSL model f_θ of GeSSL

for each task **do**

Sample a mini-batch \mathcal{B}_x from \mathcal{D}

Apply random data augmentations to \mathcal{B}_x , obtaining $\mathcal{A} = \{a^j(x_i)\}_{i=1, j=1}^{i=B, j=2}$

Regard each view $a^j(x_i)$ of the same x_i with the same pseudo-label y_i , obtaining $\mathcal{D}_x = (\mathcal{X}, \mathcal{Y})$ where $\mathcal{X} = \{a^j(x_i)\}_{i=1, j=1}^{i=B, j=2}$ are the samples and $\mathcal{Y} = \{y_i\}_{i=1}^B$ are the corresponding labels

Obtain a B -class classification task \mathcal{T}_x of each training batch \mathcal{B}_x

end for

for n tasks **do**

for $k=1, \dots, K$ **do**

Update f_θ^l using Eq.6

end for

Obtain the task-specific model f_θ^l for \mathcal{T}_x^l

Obtain the probabilistic distribution $\pi_{f_\theta^l}$ of f_θ^l

$f_\theta^{l(K)} \leftarrow f_\theta^l$

for $\iota=1, \dots, \lambda - 1$ **do**

Update $f_\theta^{l(K+\iota)}$ from $f_\theta^{l(K)}$ with further $\lambda - 1$ steps using Eq.6

end for

$\tilde{f}_\theta^l \leftarrow f_\theta^{l(K+\lambda)}$

Obtain the self-motivated target \tilde{f}_θ^l for \mathcal{T}_x^l

Obtain the probabilistic distribution $\pi_{\tilde{f}_\theta^l}$ of \tilde{f}_θ^l

Update f_θ using Eq.7:

$f_\theta \leftarrow f_\theta - \beta \sum_{\mathcal{T}_x^l \in \mathcal{T}_x} \nabla_{f_\theta} \mathcal{L}(f_\theta^l; \mathcal{D}_x^l)$

end for

A. Pseudo-code

The pseudo-code of our proposed GeSSL is shown in Algorithm 1. GeSSL is a novel self-supervised learning framework that explicitly models generality into the learning objective. It learns general knowledge through a bi-level optimization over a set of SSL tasks (see Subsection 3.2 in the main text), and update through the optimal direction towards generality guided by the proposed self-motivated target. GeSSL can be applied to any self-supervised learning model, unleashing the models' potential. It is worth noting that in our task construction process, we treat one batch of training from the original self-supervised learning framework as a multi-classification task. Then, we construct n self-supervised learning tasks based on the training data of n batches, and update the self-supervised model f_θ in GeSSL based on these n tasks simultaneously.

B. Proofs

This section provides the complete proof of Theorem 5.1 and Theorem 5.2 described in Section 5 of the main text.

B.1. Proof of Theorem 5.1

We start by proving Approximate View-Invariance illustrated in Theorem 5.1, which covers data augmentation and perspective invariance in self-supervised learning and self-supervised task construction.

Theorem B.1. (Approximate View-Invariance): The best estimate of the label y is approximately invariant to the choice of different augmented views $a^j(x)$, $j = 1, 2$ of the same x . Each target function $f_\theta : \mathcal{A} \rightarrow \mathbb{R}^n$ satisfies:

$$\mathbb{E}_{p_+(a^1(x), a^2(x))} [(f_\theta(a^1(x)) - f_\theta(a^2(x)))^2] \leq \varepsilon \quad (12)$$

where $p_+(a^1(x), a^2(x)) = \sum_x p(a^1(x)|x)p(a^2(x)|x)p(x)$ when fixed $\varepsilon \in [0, \infty)$.

Proofs. Firstly, let's expand $(f_\theta(a^1(x)) - f_\theta(a^2(x)))^2$:

$$\begin{aligned} (f_\theta(a^1(x)) - f_\theta(a^2(x)))^2 &= f_\theta^2(a^1(x)) \\ &- 2f_\theta(a^1(x))f_\theta(a^2(x)) + f_\theta^2(a^2(x)) \end{aligned} \quad (13)$$

Taking the expectation, we have:

$$\begin{aligned} &\mathbb{E}_{p_+(a^1(x), a^2(x))} [(f_\theta(a^1(x)) - f_\theta(a^2(x)))^2] \\ &= \mathbb{E}_{p_+(a^1(x), a^2(x))} [f_\theta^2(a^1(x))] \\ &- 2\mathbb{E}_{p_+(a^1(x), a^2(x))} [f_\theta(a^1(x))f_\theta(a^2(x))] \\ &+ \mathbb{E}_{p_+(a^1(x), a^2(x))} [f_\theta^2(a^2(x))] \end{aligned} \quad (14)$$

Using the linearity of the expectation operator, we can move the operator to each term. Next, we simplify the cross term

$f_\theta(a^1(x))f_\theta(a^2(x))$ by introducing an auxiliary variable $z = f_\theta(a^1(x)) - f_\theta(a^2(x))$, giving:

$$\begin{aligned} &\mathbb{E}_{p_+(a^1(x), a^2(x))} [(f_\theta(a^1(x)) - f_\theta(a^2(x)))^2] \\ &= \mathbb{E}_{p_+(a^1(x), a^2(x))} [z^2] \end{aligned} \quad (15)$$

Then, using z^2 and its expectation being less than or equal to ε :

$$\mathbb{E}_{p_+(a^1(x), a^2(x))} [z^2] \leq \varepsilon \quad (16)$$

Therefore, we have proven that the expected value in the Theorem 1 is less than or equal to ε , i.e., with different augmented views $a^1(x)$ and $a^2(x)$ of the same input x , the expected square error of the output is bounded, denoted as $\mathbb{E}_{p_+(a^1(x), a^2(x))} [(f_\theta(a^1(x)) - f_\theta(a^2(x)))^2] \leq \varepsilon$.

B.2. Proof of Theorem 5.2

Next, we proceed to the proof of Theorem 5.2, which covers the performance guarantee of GeSSL that is conducted based on Definition 4.1 and 4.2.

Theorem B.2. (Performance Guarantee) Let \tilde{f}_θ^l and f_θ^l be SSL models before and after learning general knowledge based on the proposed self-motivated target (Eq.7), $\mu_{KL}^f(\theta_1, \theta_2) = \mu_{KL}(\pi_{\tilde{f}_{\theta_1}}, \pi_{\tilde{f}_{\theta_2}})$ is also the calculation of Kullback-Leibler Divergence, the update process based on self-motivated target for each task satisfies:

$$\begin{aligned} \tilde{f}_\theta - f_\theta &= \frac{\beta}{\alpha} \mu_{KL}^f(\tilde{f}_\theta^l, f_\theta^l) - \alpha \mathcal{G}^T g \\ &- \frac{\beta}{\alpha} \mu_{KL}^f(\tilde{f}_\theta^l, f_\theta^l) + o(\beta(\alpha + \beta)) \end{aligned} \quad (17)$$

where $\mathcal{G}^T = \mathcal{M}^T \mathcal{M} \in \mathbb{R}^{n_\theta \times n_\theta}$ with the (transposed) Jacobian \mathcal{M} of f_θ^l , i.e., $\mathcal{M} := \left[\frac{\partial \theta^l}{\partial \theta} \right] \in \mathbb{R}^{n_\theta \times n_\theta}$. Note that $\nabla_{f_\theta} f_\theta^l = \mathcal{M} \nabla_{f_\theta^l} f_\theta^l$. When β sufficiently small, there exists infinitely many σ for which $\tilde{f}_\theta - f_\theta \leq 0$. The self-motivated target σ yields improvements

$$\tilde{f}_\theta - f_\theta = -\frac{\beta}{\alpha} \mu_{KL}^f(\tilde{f}_\theta^l, f_\theta^l) + o(\beta(\alpha + \beta)) \leq 0 \quad (18)$$

Proofs. To facilitate the proof, we first introduce some useful notations. We let:

$$\begin{aligned} g &= \nabla_{f_\theta} \ell(f_\theta; \mathcal{D}_x^l) \\ \mathcal{G}^T g &= f_\theta - \alpha \nabla_{f_\theta} \ell(f_\theta; \mathcal{D}_x^l) \\ \mathcal{Q}\mu &= \sum_{\mathcal{T}_x^l \in \mathcal{T}_x} \nabla_{f_\theta} \mathcal{L}(f_\theta; \mathcal{D}_x^l) \end{aligned} \quad (19)$$

Then we get $\tilde{f}_\theta = f_\theta - \beta \mathcal{Q}\mu$, by first-order Taylor series expansion of the SSL model with respect to f_θ around \tilde{f}_θ :

$$\begin{aligned} \tilde{f}_\theta &= f_\theta + \beta \langle \mathcal{Q}g, \tilde{f}_\theta - f_\theta \rangle + o(\beta^2 \|\mathcal{Q}\mu\|_2^2) \\ &= f_\theta - \beta \langle \mathcal{Q}g, \mathcal{Q}\mu \rangle + o(\beta^2 \|\mathcal{Q}\mu\|_2^2) \\ &= f_\theta - \beta \langle \mu, \mathcal{G}^T g \rangle + o(\beta^2 \|\mu\|_{\mathcal{G}^T}^2) \end{aligned} \quad (20)$$

then:

$$\tilde{f}_\theta - f_\theta = -\beta \langle \mu, \mathcal{G}^T \mathbf{g} \rangle + o(\beta^2 \|\mu\|_{\mathcal{G}^T}^2) \quad (21)$$

Combining the above formulas with the first-level optimization (Eq.6) and second-level optimization (Eq.7), we can obtain:

$$\begin{aligned} & \tilde{f}_\theta - f_\theta \\ &= \beta \left(\frac{1}{\alpha} (\mu(\tilde{f}_\theta, \mathcal{G}^T \mathbf{g}) - \mu(\tilde{f}_\theta, f_\theta^l)) \right) \\ & \quad + o(\alpha\beta \|\mathbf{Qw}\|_2^2) + o(\beta^2 \|\mathbf{Q}\mu\|_2^2) \\ &= \frac{\beta}{\alpha} (\mu(\tilde{f}_\theta, \mathcal{G}^T \mathbf{g}) - \mu(\tilde{f}_\theta, f_\theta^l)) \\ & \quad + o(\alpha\beta \|\mathbf{Qw}\|_2^2 + \beta^2 \|\mathbf{Q}\mu\|_2^2) \quad (22) \\ &= \frac{\beta}{\alpha} \mu(\tilde{f}_\theta, \mathcal{G}^T \mathbf{g}) - \frac{\beta}{\alpha} \mu(\tilde{f}_\theta, f_\theta^l) \\ & \quad + o(\alpha\beta \|\mathbf{Qw}\|_2^2 + \beta^2 \|\mathbf{Q}\mu\|_2^2) \\ &\leq \frac{\beta}{\alpha} \mu(\tilde{f}_\theta, \mathcal{G}^T \mathbf{g}) - \frac{\beta}{\alpha} \mu(\tilde{f}_\theta, f_\theta^l) + o(\alpha\beta + \beta^2) \\ &= \frac{\beta}{\alpha} \mu(\tilde{f}_\theta, \mathcal{G}^T \mathbf{g}) - \frac{\beta}{\alpha} \mu(\tilde{f}_\theta, f_\theta^l) + o(\beta(\alpha + \beta)) \end{aligned}$$

The first item in this formula measures the distance between the two set of distributions $\pi_{\tilde{f}_\theta}$ (the set of self-motivated targets distributions) and π_{f_θ} (the distribution of f_θ), and the distance measures the learning effect. In our setting, the meta-objective is to minimize the distance between two distributions. Therefore, the first term can be approximately 0. Finally, residuals capture distortions due to same objective of every term in this equation. Then:

$$\begin{aligned} \tilde{f}_\theta - f_\theta &\leq 0 - \frac{\beta}{\alpha} \mu(\tilde{f}_\theta, f_\theta^l) + o(\beta(\alpha + \beta)) \\ &= \frac{\beta}{\alpha} \mu(\tilde{f}_\theta, f_\theta^l) + o(\beta(\alpha + \beta)) \quad (23) \end{aligned}$$

As α and β become small or even zero, the residuals disappear exponentially, where $o(\beta(\alpha + \beta)) \approx 0$. Then when all the above conditions are met, $f_\theta - \tilde{f}_\theta \leq 0$ which means \tilde{f}_θ achieves performance improvements over previous f_θ . So far, the performance guarantee of self-motivated meta-training is completed.

C. Implementation Details

Task Construction. We build tasks based on images with a batch size of $B = 16$. For data augmentation, we use the same data augmentation scheme as SimCLR to augment each image in the batch 5 times. In simple terms, we draw a random patch (224×224) from the original image, and then apply a random augmentation sequence composed of random horizontal flip, cropping, color jitter, etc.

Architecture and Settings. We use C4-backbone, ResNet-18, and ResNet-50 backbones as our encoders for a fair

comparison with different methods. The convolutional layers are followed by batch normalization, ReLU nonlinearity, and max pooling (strided convolution) respectively. The last layer is fed into a softmax classifier (a classification head). These architectures are pre-trained and kept fixed during training. We optimize our model with a Stochastic Gradient Descent (SGD) optimizer, setting the momentum and weight decay values to 0.9 and 10^{-4} respectively. The specific adjustments of the experimental settings corresponding to different experiments are illustrated in Subsection 6.2-Subsection 6.5 of the main text. In the ablation experiments, we adopt the experimental settings used in the corresponding dataset, i.e., the experiment of ‘‘Influence of λ ’’ is conducted on miniImageNet, so we adopt the experimental settings described in Subsection 6.5. All the experiments are performed on NVIDIA RTX 4090 GPUs.

D. Benchmark Datasets

In this section, we briefly introduce all datasets used in our experiments. In summary, the benchmark datasets can be divided into four categories: (i) for unsupervised learning, we evaluate GeSSL on six benchmark datasets, including CIFAR-10 (Krizhevsky et al., 2009), CIFAR-100 (Krizhevsky et al., 2009), STL-10 (Coates et al., 2011), Tiny ImageNet (Le & Yang, 2015), ImageNet-100 (Tian et al., 2020) and ImageNet (Deng et al., 2009); (ii) for semi-supervised learning, we evaluate GeSSL on ImageNet (Deng et al., 2009); (iii) for transfer learning, we select two scenarios: instance segmentation (PASCAL VOC (Everingham et al., 2010)) and object detection (COCO (Lin et al., 2014)) for analysis; (iv) for few-shot learning, we select three benchmarks for evaluation, including Omniglot (Lake et al., 2019), miniImageNet (Vinyals et al., 2016a), and CIFAR-FS (Bertinetto et al., 2018). The composition of the data set is as follows:

- CIFAR-10 (Krizhevsky et al., 2009) is a prevalent image classification benchmark comprising 10 classes, each containing 5000 32×32 resolution images.
- CIFAR-100 (Krizhevsky et al., 2009), another widely used image classification benchmark, consists of 100 classes, each containing 5000 images at a resolution of 32×32 .
- STL-10 (Coates et al., 2011) encompasses 10 classes with 500 training and 800 test images per class at a high resolution of 96×96 pixels. It also includes 100,000 unlabeled images for unsupervised learning.
- Tiny ImageNet (Le & Yang, 2015), a subset of ImageNet by Stanford University, comprises 200 classes, each with 500 training, 50 verification, and 50 test images.

- ImageNet-100 (Tian et al., 2020), a subset of ImageNet, includes 100 classes, each containing 1000 images.
- ImageNet (Deng et al., 2009), organized by the WordNet hierarchy, is a renowned dataset featuring 1.3 million training and 50,000 test images across 1000+ classes.
- PASCAL VOC dataset (Everingham et al., 2010), known for object classification, detection, and segmentation, encompasses 20 classes with a total of 11,530 images split between VOC 07 and VOC 12.
- COCO dataset (Lin et al., 2014), primarily used for object detection and segmentation, comprises 91 classes, 328,000 samples, and 2,500,000 labels.
- miniImageNet (Vinyals et al., 2016a) is a few-shot learning dataset that consists of 100 classes, each with 600 images. The images have a resolution of 84x84 pixels.
- Omniglot (Lake et al., 2019) is another dataset for few-shot learning, which comprises 1623 different handwritten characters from 50 different alphabets. The 1623 characters were drawn by 20 different people online using Amazon’s Mechanical Turk. Each image is paired with stroke data $[x, y, t]$ sequences and time (t) coordinates (ms).
- CIFAR-FS (Bertinetto et al., 2018) is also a dataset for few-shot learning research, derived from the CIFAR-100 dataset. It consists of 100 classes, each with a small training set of 500 images and a test set of 100 images. The images have a resolution of 32×32 pixels.
- CropDiseases (Mohanty et al., 2016) is a dataset of 24,881 images of crop pests and diseases, with 22 categories, each including different pests and diseases of 4 crops (cashew, cassava, maize, and tomato).
- ISIC (Codella et al., 2018) is a dataset of over 13,000 dermoscopic images of skin lesions, which is the largest publicly available quality-controlled archive of dermoscopic images. The dataset includes 8 common types of skin lesions, such as melanoma, basal cell carcinoma, squamous cell carcinoma, etc.
- ChestX (Wang et al., 2017) is a dataset of 112,120 chest X-ray images, with 14 common types of chest diseases, such as pneumonia, emphysema, fibrosis, etc. The dataset was collected from 30,805 unique patients (from 1992 to 2015) of the National Institutes of Health Clinical Center (NIHCC).

In addition, we further construct cross-domain few-shot learning experiments in Appendix F.3 and introduced six benchmark data sets, including:

- CUB (Welinder et al., 2010) is a dataset of 200 bird species, with 11,788 images in total and about 60 images per species. Each image has detailed annotations, including subcategory labels, 15 part locations, 312 binary attributes, and a bounding box.
- Cars (Krause et al., 2013) is a dataset of 196 car models, with 16,185 images in total and about 80 images per model. Each image has a subcategory label, indicating the manufacturer, model, and year of the car.
- Places (Zhou et al., 2017) is a dataset of 205 scene categories, with 2.5 million images in total and about 12,000 images per category. The scene categories are defined by their functions, representing the entry-level of the environment.

E. Baselines

In this section, we briefly introduce all baselines used in the experiments for comparison. We select fifteen representative self-supervised methods as baselines. These methods cover almost all the classic and SOTA self-supervised methods, including:

- SimCLR (Chen et al., 2020a) learns visual representations by contrastive learning of augmented image pairs. It uses a neural network to maximize the similarity of positive pairs and minimize the similarity of negative pairs.
- MoCo v2 (Chen et al., 2020b) improves MoCo (Chen et al., 2020b), another contrastive learning method for visual representation learning. MoCo v2 introduces a momentum encoder, a memory bank, and a shuffling BN layer to handle limited batch size and noisy negatives. MoCo v2 also adopts SimCLR’s data augmentation and loss function to boost the performance.
- BYOL (Grill et al., 2020) does not need negative pairs or a large batch size. It uses two neural networks, an online network and a target network, that learn from each other. The online network predicts the target network’s representation of an augmented image, while the target network is updated by a slow-moving average of the online network.
- SimSiam (Chen & He, 2021) simplifies BYOL by removing the momentum encoder and the prediction MLP. It consists of two Siamese networks that map an input image to a feature vector, and a small MLP head that projects the feature vector to the contrastive learning space. SimSiam applies a stop-gradient operation to one of the MLP outputs, and uses a negative

cosine similarity loss to maximize the similarity between the two outputs.

- Barlow Twins (Zbontar et al., 2021) learns representations by enforcing that the cross-correlation matrix between the outputs of two identical networks fed with different augmentations of the same image is close to the identity matrix. This encourages the networks to produce similar representations for the positive pair, while reducing the redundancy between the representation dimensions.
- DeepCluster (Caron et al., 2018) is a clustering-based method for self-supervised learning. It iteratively groups the features produced by a convolutional network into clusters, and uses the cluster assignments as pseudo-labels to update the network parameters by supervised learning. DeepCluster can discover meaningful clusters that are discriminative and invariant to transformations, and can learn competitive features for various downstream tasks.
- SwAV (Caron et al., 2020) uses online swapping of cluster assignments between multiple views of the same image to learn visual features. SwAV first computes prototypes (cluster centers) from a large set of features, and then assigns each feature to the nearest prototype. The assignments are then swapped across the views, and the network is trained to predict the swapped assignments.
- DINO (Caron et al., 2021) learns visual features by using a teacher-student architecture and a distillation loss. The teacher network is an exponential moving average of the student network, and the distillation loss makes the student features similar to the teacher features. DINO also applies a centering and sharpening operation to the teacher features, which prevents feature collapse and increases feature diversity.
- W-MSE (Ermolov et al., 2021) learns features by using a weighted mean squared error (MSE) loss, which assigns higher weights to the informative and less noisy features, and lower weights to the less informative and more noisy features.
- RELIC v2 (Tomasev et al., 2022) learns visual features by predicting relative location of image patches. RELIC v2 divides an image into a grid of patches, and randomly selects a query and a target patch. The network is trained to predict the relative location of the target patch with respect to the query patch, using a cross-entropy loss.
- LMCL (Chen et al., 2021) learns visual features by using a large margin cosine loss (LMCL). LMCL is a metric learning loss that makes the features of the

same class closer and the features of different classes farther in the cosine space.

- ReSSL (Zheng et al., 2021) learns visual features by using a reconstruction loss and a contrastive loss. ReSSL applies random cropping and resizing to generate two views of the same image, and then feeds them to a reconstruction network and a contrastive network. The reconstruction network is trained to reconstruct the original image from the cropped view, while the contrastive network is trained to maximize the similarity between the features of the two views.
- SSL-HSIC (Li et al., 2021b) learns visual features by using a Hilbert-Schmidt independence criterion (HSIC) loss. HSIC is a measure of statistical dependence between two random variables, and can be used to align the features of different views of the same image.
- CorInfoMax (Ozsoy et al., 2022) learns visual features by maximizing the correlation and mutual information between the features of augmented image pairs and the image labels. CorInfoMax aims to learn features that are both discriminative and consistent, and outperform previous methods on image classification and segmentation tasks.
- MEC (Liu et al., 2022a) is a clustering algorithm that can handle large-scale data with limited memory by using a memory-efficient clustering (MEC) loss. MEC first samples a subset of features, and then performs k-means clustering on the subset. The cluster assignments are then propagated to the rest of the features by a nearest neighbor search.
- VICRegL (Bardes et al., 2022) learns visual features by using a variance-invariance-covariance regularization loss (VICRegL).

In addition, for the few-shot learning scenario, we choose six advanced unsupervised few-shot learning methods as comparison baselines.

- CACTUs (Hsu et al., 2018) uses clustering and augmentation to create pseudo-labels for unlabeled data. It then trains a classifier on the labeled data and fine-tunes it on a few labeled examples from the target task.
- UMTRA (Khodadadeh et al., 2019) uses random selection and augmentation to create tasks with pseudo-labels from unlabeled data. It then trains a classifier on each task and adapts it to the target task using a few labeled examples.
- LASIUM (Khodadadeh et al., 2020) uses latent space interpolation to generate tasks with pseudo-labels from

a generative model. It then trains an energy-based model on each task and adapts it to the target task using a few labeled examples.

- SVEBM (Kong et al., 2021) uses a symbol-vector coupling energy-based model to learn from unlabeled data. It then adapts the model to the target task using a diffusion process.
- GMVAE (Lee et al., 2021) uses a Gaussian mixture variational autoencoder to perform learning, and then adapts the model to the target task using a variational inference process.
- PsCo (Jang et al., 2023) uses a probabilistic subspace clustering model to learn from unlabeled data. It then adapts the model to the target task using a few labeled examples and a subspace alignment process.

F. Additional Experiments

In this section, we introduce the additional experiments, full results, and experimental details of the comparison experiments, including unsupervised learning (Appendix F.1, also Section 6.2 of the main text), transfer learning (Appendix F.2, also Section 6.4 of the main text), and few-shot learning (Appendix F.3, also Section 6.5 of the main text). Next, we conduct experiments based on the proposed σ -measure (Definition 4.2) to evaluate the generality of existing SSL methods in Appendix F.4. Finally, we apply our method to the generative self-supervised learning task and other modalities, e.g., text, to further evaluate the effectiveness of GeSSL in Appendix F.5 and Appendix F.6.

F.1. Unsupervised Learning

In this section, we present additional results of the unsupervised learning experiments. Specifically, Table 7 provides the comparison results of our proposed GeSSL on a medium-scale dataset, i.e., ImageNet-100. The results still demonstrate the proposed GeSSL’s ability to enhance the performance of self-supervised learning methods, achieving significant improvements over the original models on all baselines. Table 8 provides the comparison results of our proposed GeSSL on a large-scale dataset, i.e., ImageNet. The results show that, (i) the self-supervised learning model applying GeSSL achieves the state-of-the-art result (SOTA) performance under all epoch conditions; and (ii) after applying the proposed GeSSL, the self-supervised learning models consistently outperforms the original frameworks in terms of average classification accuracy at 100, 200 and 400 epochs. For 1000 epochs, VICRegL + GeSSL yields the best result among other state-of-the-art methods, with an average accuracy of 78.72%.

Table 7. The Top-1 and Top-5 classification accuracies of linear classifier on ImageNet-100 with ResNet-50 as feature extractor.

Method	Top-1	Top-5
SimCLR (Chen et al., 2020a)	70.15 ± 0.16	89.75 ± 0.14
MoCo (Chen et al., 2020b)	72.80 ± 0.12	91.64 ± 0.11
BYOL (Grill et al., 2020)	71.48 ± 0.15	92.32 ± 0.14
SimSiam (Chen & He, 2021)	73.01 ± 0.21	92.61 ± 0.27
Barlow Twins (Zbontar et al., 2021)	75.97 ± 0.23	92.91 ± 0.19
SwAV (Caron et al., 2020)	75.78 ± 0.16	92.86 ± 0.15
DINO (Caron et al., 2021)	75.43 ± 0.18	93.32 ± 0.19
W-MSE (Ermolov et al., 2021)	76.01 ± 0.27	93.12 ± 0.21
RELIC v2 (Tomasev et al., 2022)	75.88 ± 0.15	93.52 ± 0.13
LMCL (Chen et al., 2021)	75.89 ± 0.19	92.89 ± 0.28
ReSSL (Zheng et al., 2021)	75.77 ± 0.21	92.91 ± 0.27
SSL-HSIC (Li et al., 2021b)	74.99 ± 0.19	93.01 ± 0.20
CorInfoMax (Ozsoy et al., 2022)	75.54 ± 0.20	92.23 ± 0.25
MEC (Liu et al., 2022a)	75.38 ± 0.17	92.84 ± 0.20
VICRegL (Bardes et al., 2022)	75.96 ± 0.19	92.97 ± 0.26
SimCLR + GeSSL	72.43 ± 0.18	91.87 ± 0.21
MoCo + GeSSL	73.78 ± 0.19	93.28 ± 0.23
SimSiam + GeSSL	75.48 ± 0.19	94.83 ± 0.31
Barlow Twins + GeSSL	76.83 ± 0.19	93.23 ± 0.18
SwAV + GeSSL	76.38 ± 0.20	95.47 ± 0.19
DINO + GeSSL	76.84 ± 0.25	94.98 ± 0.24
LMCL + GeSSL	77.38 ± 0.21	95.10 ± 0.25
ReSSL + GeSSL	76.98 ± 0.23	94.88 ± 0.24
VICRegL + GeSSL	77.58 ± 0.22	95.46 ± 0.15

More recent methods The effect of GeSSL is reflected in the performance improvement when applying it to the SSL baselines. The experimental results above have demonstrated that after the introduction of GeSSL, the effects of all SSL baselines have been significantly improved. These results have shown the outstanding effectiveness and robustness of GeSSL. The SSL baselines we use cover all SOTA methods on the leaderboard of the adopted benchmark datasets (before submission). The methods proposed in 2023-24 mainly are variants of the currently used comparison baselines.

To evaluate the effect of GeSSL on recently proposed methods, we select the two SSL methods published in ICML23 for testing (Baevski et al., 2023; Joshi & Mirzasoleiman, 2023), where we follow the same experimental settings. The results are shown in Tables 12 and 13. The results still prove the effectiveness of GeSSL. We will supplement these results in the final version.

F.2. Transfer Learning

As mentioned in the Section 6.4, we construct three sets of transfer learning experiments, including the most commonly used object detection and instance segmentation protocol (Chen et al., 2020a; Zbontar et al., 2021; Grill et al., 2020), transfer to other domains (different datasets), and transfer learning on video-based tasks. The results of the first experiment are illustrated in Section 6.4, and the other two sets of experiments are described below.

Table 8. The Top-1 and Top-5 classification accuracies of linear classification on the ImageNet dataset with ResNet-50 as the feature extractor. We record the comparison results from 100, 200, 400, and 1000 epochs.

Method	100 Epochs		200 Epochs		400 Epochs	1000 Epochs
	Top-1	Top-5	Top-1	Top-5	Top-1	Top-1
Supervised	71.93	-	73.45	-	74.92	76.35
SimCLR (Chen et al., 2020a)	66.54 ± 0.22	88.14 ± 0.26	68.32 ± 0.31	89.76 ± 0.23	69.24 ± 0.21	70.45 ± 0.30
MoCo (Chen et al., 2020b)	64.53 ± 0.25	86.17 ± 0.11	67.55 ± 0.27	88.42 ± 0.11	69.76 ± 0.14	71.16 ± 0.23
BYOL (Grill et al., 2020)	67.65 ± 0.27	88.95 ± 0.11	69.94 ± 0.21	89.45 ± 0.27	71.85 ± 0.12	73.35 ± 0.27
SimSiam (Chen & He, 2021)	68.14 ± 0.26	87.12 ± 0.26	70.02 ± 0.14	88.76 ± 0.23	70.86 ± 0.34	71.37 ± 0.22
Barlow Twins (Zbontar et al., 2021)	67.24 ± 0.22	88.66 ± 0.19	69.94 ± 0.32	88.97 ± 0.27	70.22 ± 0.15	73.29 ± 0.13
SwAV (Caron et al., 2020)	66.55 ± 0.27	88.42 ± 0.22	69.12 ± 0.24	89.38 ± 0.20	70.78 ± 0.34	75.32 ± 0.11
DINO (Caron et al., 2021)	67.23 ± 0.19	88.48 ± 0.21	70.58 ± 0.24	91.32 ± 0.27	71.98 ± 0.26	73.94 ± 0.29
W-MSE (Ermolov et al., 2021)	67.48 ± 0.29	90.39 ± 0.27	70.85 ± 0.31	91.57 ± 0.20	72.49 ± 0.24	72.84 ± 0.18
RELIC v2 (Tomasev et al., 2022)	66.38 ± 0.23	90.89 ± 0.21	70.98 ± 0.21	91.15 ± 0.26	71.84 ± 0.21	72.17 ± 0.20
LMCL (Chen et al., 2021)	66.75 ± 0.13	89.85 ± 0.36	70.83 ± 0.26	90.04 ± 0.21	72.53 ± 0.24	72.97 ± 0.29
ReSSL (Zheng et al., 2021)	67.41 ± 0.27	90.55 ± 0.23	69.92 ± 0.24	91.25 ± 0.12	72.46 ± 0.29	72.91 ± 0.30
CorInfoMax (Ozsoy et al., 2022)	70.13 ± 0.12	91.14 ± 0.25	70.83 ± 0.15	91.53 ± 0.22	73.28 ± 0.24	74.87 ± 0.36
MEC (Liu et al., 2022a)	69.91 ± 0.10	90.67 ± 0.15	70.34 ± 0.27	91.25 ± 0.38	72.91 ± 0.27	75.07 ± 0.24
VICRegL (Bardes et al., 2022)	69.99 ± 0.25	91.27 ± 0.16	70.24 ± 0.27	91.60 ± 0.24	72.14 ± 0.20	75.07 ± 0.23
SimCLR + GeSSL	68.38 ± 0.18	89.74 ± 0.22	69.65 ± 0.16	90.98 ± 0.19	71.30 ± 0.19	72.48 ± 0.29
MoCo + GeSSL	66.54 ± 0.22	88.19 ± 0.23	69.47 ± 0.28	90.34 ± 0.28	70.48 ± 0.30	72.81 ± 0.21
SimSiam + GeSSL	70.48 ± 0.19	88.34 ± 0.17	71.74 ± 0.19	89.28 ± 0.30	72.58 ± 0.18	74.55 ± 0.25
Barlow Twins + GeSSL	69.39 ± 0.20	89.40 ± 0.21	71.89 ± 0.22	90.32 ± 0.14	73.90 ± 0.19	74.91 ± 0.23
SwAV + GeSSL	68.93 ± 0.19	89.39 ± 0.16	71.47 ± 0.10	90.28 ± 0.28	72.48 ± 0.19	76.15 ± 0.18
DINO + GeSSL	69.39 ± 0.19	90.49 ± 0.21	72.84 ± 0.19	93.54 ± 0.18	73.84 ± 0.28	76.15 ± 0.20
VICRegL + GeSSL	72.38 ± 0.23	91.23 ± 0.19	73.54 ± 0.29	93.17 ± 0.30	74.15 ± 0.25	78.72 ± 0.29

Table 9. The performance of adding task information in self-supervised models on different datasets.

Evl.dataset	SimCLR+GeSSL	BYOL+GeSSL	Barlow Twins+GeSSL
CIFAR10	+3.51	+2.49	+2.12
Flower102	+3.99	+2.05	+2.96
Food101	+1.81	+2.35	+1.96
Aircraft	+2.55	+2.86	+2.19

Transfer to other domains. To explore the nature of transfer learning of the proposed framework, we leverage models that had been pre-trained on the CIFAR100 dataset, including SimCLR (Chen et al., 2020a), BYOL (Grill et al., 2020), and Barlow Twins (Zbontar et al., 2021), on the CIFAR100 dataset. We then applied these models to four distinct datasets, including CIFAR10 (Krizhevsky et al., 2009), Flower102 (Nilsback & Zisserman, 2008), Food101 (Bossard et al., 2014), and Aircraft (Maji et al., 2013). We first calculate the classification performance (Top-1) based on the existing self-supervised model on different data sets, recorded as $acc(\text{method}, \text{dataset})$, such as $acc(\text{SimCLR}, \text{Flower102})$. Then, we calculate the model’s classification performance by incorporating GeSSL on those data sets, which is recorded as $acc(\text{method} + \text{GeSSL}, \text{dataset})$. Finally, we get the improvement $\Delta(\text{method}, \text{dataset}) = acc(\text{method} + \text{GeSSL}, \text{dataset}) - acc(\text{method}, \text{dataset})$

in classification performance on each dataset, as shown in Table 9. The results show that the migration effect of the model after applying the GeSSL framework has been steadily improved, proving that GeSSL has effectively improved the versatility of the SSL model.

Video-based Task In order to assess the performance of our method with video-based tasks, we transition our pre-trained model to handle a variety of video tasks, utilizing the UniTrack evaluation framework (Wang et al., 2021) as our testing ground. The findings are compiled in Table 10, which includes results from five distinct tasks, drawing on the features from [layer3/layer4] of the Resnet-50. The data indicates that existing SSL methods incorporating our GeSSL significantly surpass original SSL approaches, with SimCLR achieving more than a 2% improvement in VOS (Perazzi et al., 2016), and BYOL seeing over a 3% gain in MOT (Milan et al., 2016).

F.3. Few-shot Learning

The outstanding performance of GeSSL in the few-shot learning scenario has been confirmed in Subsection 6.5, where it can produce good results with limited data. However, the situation becomes complicated in scenarios where data collection is infeasible in real life, such as medical diagnosis and satellite imagery (Zheng, 2015; Tang et al., 2012).

Table 10. Transfer learning on video tracking tasks. All methods use the same ResNet-50 backbone and are evaluated based on UniTrack.

Method	SOT		VOS	MOT		MOTS		PoseTrack
	AUC _{XCorr}	AUC _{DCF}	\mathcal{J} -mean	IDF1	HOTA	IDF1	HOTA	IDF1
SimCLR	47.3 / 51.9	61.3 / 50.7	60.5 / 56.5	66.9 / 75.6	57.7 / 63.2	65.8 / 67.6	67.7 / 69.5	72.3 / 73.5
MoCo	50.9 / 47.9	62.2 / 53.7	61.5 / 57.9	69.2 / 74.1	59.4 / 61.9	70.6 / 69.3	71.6 / 70.9	72.8 / 73.9
SwAV	49.2 / 52.4	61.5 / 59.4	59.4 / 57.0	65.6 / 74.4	56.9 / 62.3	68.8 / 67.0	69.9 / 69.5	72.7 / 73.6
BYOL	48.3 / 55.5	58.9 / 56.8	58.8 / 54.3	65.3 / 74.9	56.8 / 62.9	70.1 / 66.8	70.8 / 69.3	72.4 / 73.8
Barlow Twins	44.5 / 55.5	60.5 / 60.1	61.7 / 57.8	63.7 / 74.5	55.4 / 62.4	68.7 / 67.4	69.5 / 69.8	72.3 / 74.3
SimCLR+GeSSL	50.3 / 54.0	63.1 / 53.7	62.6 / 58.5	69.7 / 77.7	60. / 65.2	67.8 / 69.9	69.0 / 71.3	73.4 / 74.5
BYOL+GeSSL	51.5 / 57.4	60.3 / 58.9	60.7 / 57.0	67.4 / 76.9	57.9 / 64.2	72.5 / 68.3	73.2 / 71.3	74.7 / 75.3

Therefore, the performance of the model on cross-domain few-shot learning tasks is crucial, as it determines the applicability of the learning model (Guo et al., 2020). To ensure that GeSSL can achieve robust performance in real-world applications, we further conduct comparative experiments on cross-domain few-shot learning.

Experimental setup. We compare our proposed GeSSL with the few-shot learning baselines as described in Table 5 (Subsection 6.5) on cross-domain few-shot learning. The details of the baselines are illustrated in Appendix E. We adopt six cross-domain few-shot learning benchmark datasets, and divided these datasets into two categories according to their similarity with ImageNet: i) high similarity: CUB (Welinder et al., 2010), Cars (Krause et al., 2013), and Places (Zhou et al., 2017); ii) low similarity: CropDiseases (Mohanty et al., 2016), ISIC (Codella et al., 2018), and ChestX (Wang et al., 2017). The (N, K) in the tables means the N -way K -shot tasks with N classes and $N \times K$ samples, where each class has K samples augmented from the same image.

Results. Table 11 presents the performance of the model trained on miniImageNet and transfer to the six cross-domain few-shot learning benchmark datasets mentioned above. By observation, we further validate the performance of our proposed GeSSL: i) Effectiveness: achieves better results than the state-of-the-art baselines on almost all benchmark datasets; ii) Generalization: achieves nearly a 3% improvement compared to unsupervised few-shot Learning and self-supervised learning on the datasets with significant differences from the training phase; iii) Robustness: achieves better results than the PsCo (Jang et al., 2023) which introduces out-of-distribution samples, even though we do not explicitly consider out-of-distribution samples on datasets with significant differences.

F.4. Generality of Existing SSL Methods

Current self-supervised learning (SSL) models overlook the explicit incorporation of generality within their objectives, and the corresponding theoretical comprehension remains inadequate, posing challenges for SSL models to attain generality in practical, real-world applications (Huang et al.,

2021; Sun et al., 2020; Ericsson et al., 2022).

Therefore, we propose a provable σ -measure (Definition 4.2) in Section 4.2 to help evaluate the model generality, and further build GeSSL based on it to explicitly model generality into the SSL’s learning objective. In this subsection, we specifically quantify the generality scores of existing SSL methods based on σ -measure, and verify that our proposed GeSSL actually improves the model generality.

Specifically, we chose two scenarios based on images and videos to evaluate the model versatility following (Liu et al., 2022b). The image-based tasks include linear probing (top-1 accuracy) with 800-epoch pre-trained models (LIN), semi-supervised classification (top-1 accuracy) using 1% subset of training data (SEMI), object detection (AP) on VOC dataset (VOC) and COCO dataset (COCO), instance segmentation (AP^{mask}) on COCO dataset (SEG). For video-based tasks, we compute rankings in terms of AUC for SOT, \mathcal{J} -mean for VOS, IDF-1 for MOT, IDF-1 for PoseTracking, and IDF-1 for MOTS, respectively. Next, we evaluate the σ -measurement scores of different baselines before and after the introduction of GeSSL and after training for 200 epochs. Among them, the better model is set to the result of ground truth, and the calculation of σ -measurement score is performed on a series of randomly sampled tasks. Figure 5 shows the comparison results. Note that the lower σ -measure denotes the better performance. From the results, we can observe that: (i) the σ -measurement score of the existing SSL model is low and it is difficult to achieve good results in multiple domains and tasks; (ii) after the introduction of GeSSL, the σ -measurement score of the SSL models are significantly decreased. The results demonstrated that the existing SSL model has limited generality (proves the description in Section 1), and the performance improvement brought by GeSSL is achieved by improving the generality.

Considering that the above experiments evaluate the evaluation generality of SSL models, here, we construct the following numerical experiments to evaluate learning generality: In the first 20-200 epochs of training (each epoch contains multiple tasks), we evaluate the average perfor-

Table 11. The cross-domain few-shot learning accuracies ($\pm 95\%$ confidence interval). We transfer models trained on miniImageNet to six benchmark datasets with the C4-backbone. The best results are highlighted in **bold**. The (N, K) means the N -way K -shot tasks with N classes and $N \times K$ samples, where each class has K samples augmented from the same image.

Method	CUB		Cars		Places	
	(5,5)	(5,20)	(5,5)	(5,20)	(5,5)	(5,20)
<i>Unsupervised Few-shot Learning</i>						
MetaSVEBM	45.893 \pm 0.334	54.823 \pm 0.347	33.530 \pm 0.367	44.622 \pm 0.299	50.516 \pm 0.397	61.561 \pm 0.412
MetaGMVAE	48.783 \pm 0.426	55.651 \pm 0.367	30.205 \pm 0.334	39.946 \pm 0.400	55.361 \pm 0.237	65.520 \pm 0.374
PsCo	56.365 \pm 0.636	69.298 \pm 0.523	44.632 \pm 0.726	56.990 \pm 0.551	64.501 \pm 0.780	73.516 \pm 0.499
<i>Self-supervised Learning</i>						
SimCLR	51.389 \pm 0.365	60.011 \pm 0.485	38.639 \pm 0.432	52.412 \pm 0.783	59.523 \pm 0.461	68.419 \pm 0.500
MoCo	52.843 \pm 0.347	61.204 \pm 0.429	39.504 \pm 0.489	50.108 \pm 0.410	60.291 \pm 0.583	69.033 \pm 0.654
SwAV	51.250 \pm 0.530	61.645 \pm 0.411	36.352 \pm 0.482	51.153 \pm 0.399	58.789 \pm 0.403	68.512 \pm 0.466
SimCLR + GeSSL	55.541 \pm 0.456	64.489 \pm 0.198	43.656 \pm 0.199	55.841 \pm 0.248	64.846 \pm 0.300	72.651 \pm 0.244
MoCo + GeSSL	57.485 \pm 0.235	65.348 \pm 0.279	45.348 \pm 0.319	55.094 \pm 0.248	66.489 \pm 0.198	73.983 \pm 0.251
SwAV + GeSSL	55.289 \pm 0.190	65.839 \pm 0.498	42.015 \pm 0.315	56.481 \pm 0.420	64.452 \pm 0.350	72.237 \pm 0.481
Method	CropDiseases		ISIC		ChestX	
	(5,5)	(5,20)	(5,5)	(5,20)	(5,5)	(5,20)
<i>Unsupervised Few-shot Learning</i>						
MetaSVEBM	71.652 \pm 0.837	84.515 \pm 0.902	37.106 \pm 0.732	48.001 \pm 0.723	27.238 \pm 0.685	29.652 \pm 0.610
MetaGMVAE	72.683 \pm 0.527	80.777 \pm 0.511	30.630 \pm 0.423	37.574 \pm 0.399	24.522 \pm 0.405	26.239 \pm 0.422
PsCo	89.565 \pm 0.372	95.492 \pm 0.399	43.632 \pm 0.400	54.886 \pm 0.359	21.907 \pm 0.258	24.182 \pm 0.389
<i>Self-supervised Learning</i>						
SimCLR	80.360 \pm 0.488	89.161 \pm 0.456	44.669 \pm 0.510	51.823 \pm 0.411	26.556 \pm 0.385	30.982 \pm 0.422
MoCo	81.606 \pm 0.485	90.366 \pm 0.377	44.328 \pm 0.488	52.398 \pm 0.396	24.198 \pm 0.400	27.893 \pm 0.412
SwAV	80.055 \pm 0.502	89.917 \pm 0.539	43.200 \pm 0.356	50.109 \pm 0.350	21.252 \pm 0.439	28.270 \pm 0.417
SimCLR + GeSSL	84.298 \pm 0.428	94.438 \pm 0.348	47.546 \pm 0.402	55.486 \pm 0.345	30.560 \pm 0.277	34.343 \pm 0.415
MoCo + GeSSL	85.667 \pm 0.374	95.520 \pm 0.345	46.437 \pm 0.347	56.676 \pm 0.280	29.258 \pm 0.344	31.468 \pm 0.290
SwAV + GeSSL	85.274 \pm 0.345	94.667 \pm 0.350	46.463 \pm 0.291	55.203 \pm 0.317	27.237 \pm 0.355	32.130 \pm 0.211

Table 12. Top-1 validation accuracy on ImageNet-1K dataset for two settings, i.e., ViT-B and ViT-L.

Method	Epoch	ViT-B	ViT-L
data2vec 2.0	200/150	80.5	81.8
data2vec 2.0 + GeSSL	200/150	85.2	86.7

Table 13. Downstream classification accuracy of SimCLR-SAS on CIFAR-10.

Method	Subset Size	Top-1 Accuracy (%)
SimCLR-SAS	10%	79.7
SimCLR-SAS + GeSSL	10%	82.0

mance of multiple f_{θ}^l in each epoch. Each f_{θ}^l is obtained by updating f_{θ} on the corresponding training tasks **with one step**. We calculate the accuracy of SimCLR before and after the introduction of GeSSL and the ratio r of their effects on the CIFAR-10 data set. If $r < 1$, it means that the representation effect learned by the model in each epoch of training is better when introducing GeSSL. The results for every 20 epochs are shown in the table below. The results show that: (i) r is always less than 1, which proves that the repre-

sentation effect learned after the introduction of GeSSL is significantly improved; (ii) after the introduction of GeSSL, the accuracy of the model is significantly improved, and it becomes stable after 80 epochs, i.e., great results can be achieved for even based on just one iteration and few data. These results show that "the model f_{θ} achieves comparable performance on each task quickly with few data during training" after introducing GeSSL.

F.5. Evaluation on Generative Self-supervised Learning

In this subsection, we evaluate the effectiveness of the proposed GeSSL on the generative self-supervised learning paradigm. Specifically, we consider the scenario of image captioning following (Mohamed et al., 2022). The dataset we use to train the pretext task is the unlabeled part of MSCOCO dataset (Vinyals et al., 2016b), which contains 123K images with an average resolution of 640×480 pixels. This dataset contains color and grayscale images. For downstream tasks, we use the Flickr8K dataset (Hodosh et al., 2013). Next, we train it using pre-trained pre-text tasks supervised by VGG-16 and ResNet-50, as well as self-supervised pre-text tasks from SimCLR and Jigsaw Puzzle

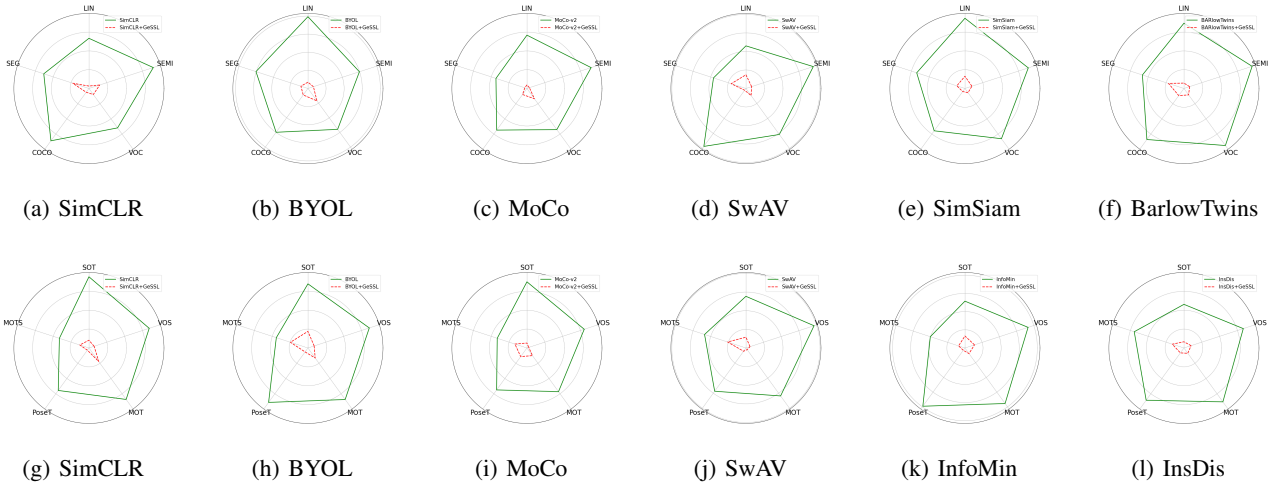


Figure 5. Generality performance of different models on five image-based tasks (top row) and five video-based tasks (bottom row). We choose σ -measure as the measurement. It is worth noting that the smaller the σ -measure score, the better the effect. Meanwhile, we normalize the results of σ -measure scores on different datasets and compare the performance between baselines by comparing the corresponding branch of the fan chart.

Table 14. The performance of introducing GeSSL during training. All results are recorded during training using the σ -measurement.

Metric	Training Epochs									
	20	40	60	80	100	120	140	160	180	200
Accuracy of SimCLR	20.1	43.6	51.2	60.2	70.3	77.2	82.3	86.1	88.7	88.6
Accuracy of SimCLR + GeSSL	41.9	66.3	82.1	93.5	93.4	93.0	93.6	93.7	93.7	93.8
Performance Ratio r	0.479	0.657	0.623	0.643	0.752	0.830	0.879	0.918	0.946	0.944

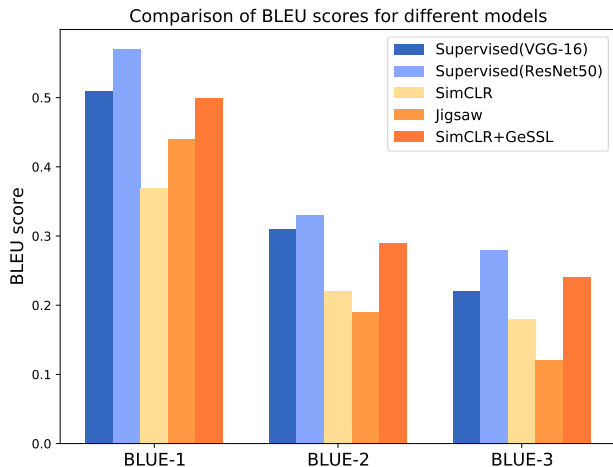


Figure 6. Comparison of BLEU scores for different models, comparing 2 fully supervised and 3 self-supervised pre-text tasks, trained on the Flickr8k.

solutions. In the next step, to evaluate the results, we use the BLEU (Bilingual Evaluation Research) score as the evaluation metric, which evaluates the generated sentences against the reference sentences, where a perfect match is 1 and a perfect mismatch is 0, calculating scores for 1, 2, 3 and 4 cumulative n-grams. The results are shown in Figure 6. From the results, we can observe that after introducing the GeSSL framework we proposed, the model effect has been further improved, stably exceeding the SOTA of the SSL method, and even approaching the supervised learning results. The results show that our proposed GeSSL can still achieve good results in generative self-supervised learning.

F.6. Evaluation on More Modalities

GeSSL proposed in this work can be applied in various fields and domains, e.g., instance segmentation, video tracking, sample generation, etc., as mentioned before. Here, we provide the experiments of GeSSL on text modality-based datasets, i.e., IC03 and IIIT5K (Yasmeen et al., 2020), which we have conducted before. We follow the same experimental settings as mentioned in (Aberdam et al., 2021). The results shown in Table 15 demonstrate that GeSSL achieves stable

Table 15. Performance on for text recognition.

Methods	IIT5K	IC03
SimCLR (Chen et al., 2020a)	1.7	3.8
SeqCLR (Aberdam et al., 2021)	35.7	43.6
SimCLR + GeSSL	19.0	19.2
SeqCLR + GeSSL	39.0	49.0

effectiveness and robustness in various modalities combined with the above experiments.

G. Details of Ablation Study

In this section, we introduce the experimental details and more comprehensive analysis of the ablation studies (Subsection 6.6), including influence of λ , model efficiency, role of loss, and implementation of bi-level optimization. In addition, we further conduct ablation experiments for task construction, and display the experimental settings and results in Appendix G.5

G.1. Influence of λ

This ablation study evaluates the effect of the hyperparameter λ in the self-motivated target. Recall that GeSSL explicitly models generality into self-supervised learning, and as mentioned in Subsection 4.1 of the main text, generality involves two aspects, including: (i) learning generality, i.e., the model f_θ which learns general representations during training, should achieve competitive performance on each task quickly with few data; (ii) evaluation generality, i.e., the trained f_θ^* , which has learned general representations, should adapt to different tasks simultaneously with minimal additional data. Therefore, we hope that GeSSL can enable the model to achieve optimal results based on few update steps. Our experimental setup constraints several conditions: (i) fast adaptation: keep the update steps K of the first-level optimization in a small range of $K \in [1, 15]$; (ii) few data: use miniImageNet as the benchmark dataset, and follow the settings of few-shot learning experiments; and (iii) performance evaluation: evaluate the effect of SimCLR + GeSSL, in addition to evaluating the accuracy under different λ , we can also compare with the results of few-shot learning experiments (Subsection 6.5 and Table 5).

The results of the ablation experiment about “influence of λ ” are presented in Table 6 of the main text. Through further analysis, we derive two additional conclusions: (i) Combining with Table 5 of the main text, regardless of the value of K , SimCLR + GeSSL consistently outperforms SimCLR on miniImageNet, demonstrating the performance enhancement brought by GeSSL; (ii) Considering Figure 2 of the main text, despite the introduction of generality con-

straints by GeSSL, the computational efficiency of SimCLR + GeSSL remains better than that of SimCLR, proving the efficiency improvement brought by GeSSL.

G.2. Model efficiency

This ablation study explores the efficiency of self-supervised models before and after applying GeSSL. Specifically, we choose five baselines, including SimCLR (Chen et al., 2020a), MOCO (Chen et al., 2020b), BYOL (Grill et al., 2020), Barlow Twins (Zbontar et al., 2021), and SwAV (Caron et al., 2020). Then, we evaluate the accuracy, training hours, and parameter size of these models on STL-10 before and after applying our proposed GeSSL. We use the same linear evaluation setting as in Subsection 6.1 of the main text. The setting for GeSSL is “K=1” and “ $\lambda = 10$ ”. Finally, we plot the trade-off scatter plot by recording the average values of five runs. The results are shown in Figure 2 of the main text, where the horizontal axis represents the training hours and the vertical axis represents the accuracy. The center of each circle represents the result of the training time and accuracy of each model, and the area of the circle represents the parameter size. The numerical results of this experiment are shown in Table 16. From the results, we can see that: (i) GeSSL can significantly improve the performance and computational efficiency of self-supervised learning models; (ii) our designed self-motivated target achieves the goal of guiding the model update towards generality with few samples and fast adaptation; (iii) although GeSSL optimizes based on bi-level optimization, the impact of the increased parameter size of GeSSL is negligible.

G.3. Role of loss

This ablation study explores the role of the loss function in the second-level optimization of GeSSL. The goal of the second-level optimization is to update the model towards generality, and the choice of loss function directly affects the model performance. Therefore, we select four commonly used loss functions, including MSE (Tsai et al., 2020), cross-entropy (De Boer et al., 2005), KL divergence (Hershey & Olsen, 2007), and Wasserstein distance (Panaretos & Zemel, 2019). We record the performance and training time of SimCLR + GeSSL with different losses on STL-10. These loss functions are computed as follows:

MSE (mean squared error) (Tsai et al., 2020) calculates the mean of the squared difference between model predictions and true values. The advantage of MSE is that it is simple to calculate, and the disadvantage is that it is sensitive to outliers. The formula for MSE is:

$$\text{MSE}(y, \hat{y}) = \frac{1}{n} \sum_{i=1}^n (y_i - \hat{y}_i)^2 \quad (24)$$

where y is the true value, \hat{y} is the predicted value, and n is

Table 16. Model analysis including parameter size, training time, and performance.

Methods	Memory Footprint (MiB)	Parameter Size (M)	Training Time (h)	Accuracy (%)
SimCLR	2415	23.15	4.15	90.5
MOCO	2519	24.01	4.96	90.9
BYOL	2691	25.84	6.98	91.9
BarlowTwins	2477	23.15	5.88	90.3
SwAV	2309	22.07	4.45	90.7
SimCLR+GeSSL	2713	26.05	3.36	93.1
MOCO+GeSSL	2801	27.01	4.17	94.2
BYOL+GeSSL	2902	28.05	5.64	94.5
BarlowTwins+GeSSL	2833	27.07	5.22	93.9
SwAV+GeSSL	2971	28.50	3.91	92.8

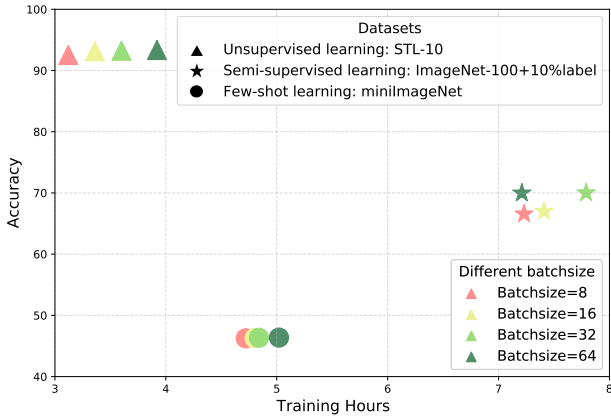


Figure 7. The effect of batchsize in SSL task construction (also the number of classes in SSL task) for GeSSL.

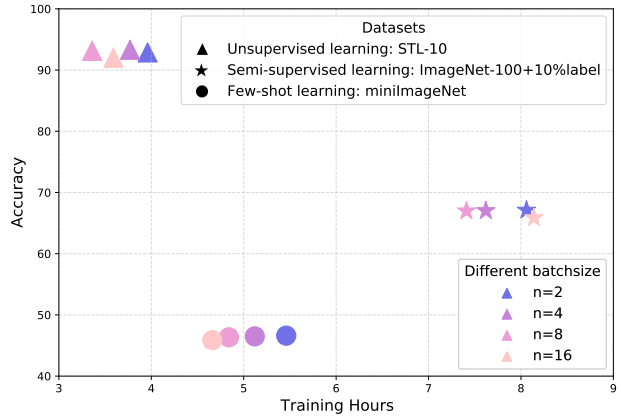


Figure 8. The effect of n in the second-level optimization (also the number of SSL tasks that are learned simultaneously) for GeSSL.

the number of samples.

Cross-entropy (De Boer et al., 2005) is a loss function used for classification problems, which calculates the difference between model-predicted probabilities and true probabilities. The advantage of cross-entropy is that it can reflect the uncertainty of the model, and the disadvantage is that it may cause the gradient to vanish or explode. The formula for cross-entropy is:

$$CE(y, \hat{y}) = - \sum_{i=1}^n y_i \log \hat{y}_i \quad (25)$$

where y is the true probability, \hat{y} is the predicted probability, and n is the number of classes.

KL divergence (Kullback-Leibler divergence) (Hershey & Olsen, 2007) is a measure of the similarity between two probability distributions, which can be seen as the difference between cross-entropy and entropy. The advantage of KL divergence is that it can reflect the distance between distributions, and the disadvantage is that it is asymmetric

and may be unbounded. The formula for KL divergence is:

$$KL(P||Q) = \sum_i P(i) \log \frac{P(i)}{Q(i)} \quad (26)$$

where P is the true distribution, Q is the predicted distribution.

Wasserstein distance (Panaretos & Zemel, 2019) is a measure of the distance between two probability distributions, which can be seen as the minimum cost of transforming one distribution into another. The advantage of Wasserstein distance is that it can reflect the geometric structure of the distributions, and the disadvantage is that it is computationally complex and requires regularization. The formula for Wasserstein distance is:

$$WD(P, Q) = \inf_{\gamma \in \Pi(P, Q)} \mathbb{E}_{(X, Y) \sim \gamma} [\|X - Y\|] \quad (27)$$

where P is the true distribution, Q is the predicted distribution, $\Pi(P, Q)$ is the set of all joint distributions that couple P and Q , and $\|\cdot\|$ is some distance measure.

From empirical analysis, Figure 3 in the main text provides the experimental results. We find that GeSSL achieves the best balance between accuracy and computational efficiency when using self-motivated target with KL divergence, i.e., the model achieves the highest accuracy in the shortest training time. Specifically, whether from the accuracy or the computational efficiency, applying KL divergence to evaluate the distribution difference and then update the model is much more efficient than applying MSE and cross-entropy losses. Although applying Wasserstein distance achieves similar accuracy, its computational time is significantly larger than applying KL divergence. Thus, we use KL divergence to optimize our model in the second-level optimization.

From theoretical analysis, the superiority of KL divergence is reflected in three aspects (Hershey & Olsen, 2007; Goldberger et al., 2003; Shlens, 2014): (i) KL divergence is non-negative, and it is zero if and only if the two distributions are exactly the same, which is consistent with our intuitive understanding of difference (Gong et al., 2021). (ii) KL divergence is a convex function, which means that optimizing it is more likely to converge to the global optimum, rather than getting stuck in the local optimum (Hershey & Olsen, 2007). (iii) KL divergence can be seen as a generalization of information entropy, which can measure the information loss between two distributions, as well as the uncertainty of one distribution relative to another distribution (Goldberger et al., 2003). In contrast, the other three losses have some limitations in scenarios we focus on: (i) MSE is very sensitive to outliers, and not suitable for dealing with probability distributions, because it does not take into account the properties of probability, such as non-negativity and normalization (Marmolin, 1986; Chicco et al., 2021; Lebanon, 2010). (ii) cross-entropy (De Boer et al., 2005; Botev et al., 2013) can be seen as a special case of KL divergence, but when the true distribution is not a one-hot vector, it cannot reflect the difference between the two distributions, and it also cannot handle continuous probability distributions. (iii) Wasserstein distance (Panaretos & Zemel, 2019; Vallender, 1974) is a distance measure based on optimal transport theory, which can measure the shape difference between two distributions, rather than the point-to-point difference. However, it has high computational complexity, and it also requires some smoothness of the distributions. Therefore, KL divergence is more suitable for measuring the difference between probability distributions, and easier to optimize in our proposed GeSSL.

G.4. Implementation of the bi-level optimization

The model of GeSSL is updated based on bi-level optimization, and the model gradients for each level are obtained by combining the optimal response Jacobian matrices through the chain rule. In practical applications, multi-level gradi-

ent computation requires a lot of memory and computation (Choe et al., 2022), so we hope to introduce a more concise gradient backpropagation and update method to reduce the computational complexity. Specifically, we consider two types of gradient update methods, including iterative differentiation (ITD) (Finn et al., 2017) and approximate implicit differentiation (AID) (Grazzi et al., 2020). We provide implementations of four popular ITD/AID algorithms, including ITD with reverse-mode automatic differentiation (ITD-RMAD) (Finn et al., 2017), AID with Neumann series (AID-NMN) (Lorraine et al., 2020), AID with conjugate gradient (AID-CG) (Rajeswaran et al., 2019), and AID with finite difference (AID-FD) (Liu et al., 2018). We also choose the recently proposed optimizer, i.e., Lookahead (Zhang et al., 2019) for comparison. We denote the the upper-level parameters and the lower-level parameters as θ and ϕ , respectively. All the way of gradient update of the bi-level optimization are as follows:

ITD-RMAD (Finn et al., 2017), ITD with reverse-mode automatic differentiation applies the implicit function theorem to the lower-level optimization problem and computes the gradients of the upper-level objective with respect to the upper-level parameters using reverse-mode automatic differentiation. The update process is as follows:

- Solve the lower-level optimization problem $\phi^* = \arg \min_{\phi} L(\phi, \theta)$ using gradient descent.
- Compute the gradient of the upper-level objective $g(\theta) = F(\phi^*, \theta)$ with respect to θ using reverse-mode automatic differentiation:

$$\begin{aligned} \nabla_{\theta} g(\theta) &= \nabla_{\theta} F(\phi^*, \theta) \\ & - \nabla_{\phi} F(\phi^*, \theta)^T (\nabla_{\phi} L(\phi^*, \theta))^{-1} \nabla_{\theta} L(\phi^*, \theta) \end{aligned} \quad (28)$$
- Update the upper-level parameters using gradient descent or other methods: $\theta \leftarrow \theta - \alpha \nabla_{\theta} g(\theta)$.

AID-NMN (Lorraine et al., 2020), AID with Neumann series, approximates the inverse of the Hessian matrix of the lower-level objective using a truncated Neumann series expansion and computes the gradients of the upper-level objective with respect to the upper-level parameters using forward-mode automatic differentiation. The update process is as follows:

- Solve the lower-level optimization problem $\phi^* = \arg \min_{\phi} L(\phi, \theta)$ using gradient descent.
- Compute the gradient of the upper-level objective $g(\theta) = F(\phi^*, \theta)$ with respect to θ using forward-mode automatic differentiation:

$$\begin{aligned}
 \nabla_{\theta}g(\theta) &= \nabla_{\theta}F(\phi^*, \theta) \\
 &- \nabla_{\phi}F(\phi^*, \theta)^T (\nabla_{\phi}L(\phi^*, \theta))^{-1} \nabla_{\theta}L(\phi^*, \theta) \\
 &\approx \nabla_{\theta}F(\phi^*, \theta) \\
 &- \nabla_{\phi}F(\phi^*, \theta)^T \sum_{k=0}^K (-1)^k (\nabla_{\phi}^2 L(\phi^*, \theta))^k \nabla_{\theta}L(\phi^*, \theta)
 \end{aligned} \tag{29}$$

where K is the truncation order of the Neumann series.

- Update the upper-level parameters using gradient descent or other methods: $\theta \leftarrow \theta - \alpha \nabla_{\theta}g(\theta)$.

AID-CG (Rajeswaran et al., 2019), AID with conjugate gradient, solves a linear system involving the Hessian matrix of the lower-level objective using the conjugate gradient algorithm and computes the gradients of the upper-level objective with respect to the upper-level parameters using forward-mode automatic differentiation. The update process is as follows:

- Solve the lower-level optimization problem $\phi^* = \arg \min_{\phi} L(\phi, \theta)$ using gradient descent or other methods.
- Compute the gradient of the upper-level objective $g(\theta) = F(\phi^*, \theta)$ with respect to θ using forward-mode automatic differentiation:

$$\begin{aligned}
 \nabla_{\theta}g(\theta) &= \nabla_{\theta}F(\phi^*, \theta) \\
 &- \nabla_{\phi}F(\phi^*, \theta)^T (\nabla_{\phi}L(\phi^*, \theta))^{-1} \nabla_{\theta}L(\phi^*, \theta) \approx \nabla_{\theta}F(\phi^*, \theta) \\
 &- \nabla_{\phi}F(\phi^*, \theta)^T v
 \end{aligned} \tag{30}$$

where v is the solution of the linear system $(\nabla_{\phi}^2 L(\phi^*, \theta))v = \nabla_{\theta}L(\phi^*, \theta)$ obtained by the conjugate gradient algorithm.

- Update the upper-level parameters using gradient descent or other methods: $\theta \leftarrow \theta - \alpha \nabla_{\theta}g(\theta)$.

AID-FD (Liu et al., 2018), AID with finite difference, approximates the inverse of the Hessian matrix of the lower-level objective using a finite difference approximation and computes the gradients of the upper-level objective with respect to the upper-level parameters using forward-mode automatic differentiation. The update process is as follows:

- Solve the lower-level optimization problem $\phi^* = \arg \min_{\phi} L(\phi, \theta)$ using gradient descent or other methods.
- Compute the gradient of the upper-level objective $g(\theta) = F(\phi^*, \theta)$ with respect to θ using forward-mode automatic differentiation:

$$\begin{aligned}
 \nabla_{\theta}g(\theta) &= \nabla_{\theta}F(\phi^*, \theta) \\
 &- \nabla_{\phi}F(\phi^*, \theta)^T (\nabla_{\phi}L(\phi^*, \theta))^{-1} \nabla_{\theta}L(\phi^*, \theta) \\
 &\approx \nabla_{\theta}F(\phi^*, \theta) \\
 &- \nabla_{\phi}F(\phi^*, \theta)^T \frac{\nabla_{\theta}L(\phi^* + \epsilon \nabla_{\theta}L(\phi^*, \theta), \theta) - \nabla_{\theta}L(\phi^*, \theta)}{\epsilon}
 \end{aligned} \tag{31}$$

where ϵ is a small positive constant for the finite difference approximation.

- Update the upper-level parameters using gradient descent or other methods: $\theta \leftarrow \theta - \alpha \nabla_{\theta}g(\theta)$.

Lookahead (Zhang et al., 2019) introduces a novel approach to optimization by maintaining two sets of weights: the fast and the slow weights. The fast weights, θ_{fast} , are updated frequently through standard optimization techniques, while the slow weights, θ_{slow} , are updated at a lesser frequency. The key formula that updates the slow weights is given by:

$$\theta_{\text{slow}} \leftarrow \theta_{\text{slow}} + \alpha(\theta_{\text{fast}} - \theta_{\text{slow}}) \tag{32}$$

where α is a hyperparameter controlling the step size. This method aims to stabilize training and ensure consistent convergence.

The results shown in Figure 4 of the main text demonstrate that approximate implicit differentiation with finite difference also achieves optimal results on the SSL model. Our optimization process is also based on this setting.

G.5. Effect of task construction

GeSSL learns from a series of self-supervised learning tasks that are constructed based on data augmentation (Subsection 3.2 in the main text). Specifically, the augmented data from the same image have significant entity similarity, so we assign the same class label $y_j \in \mathcal{Y}$ to the augmented data from the same image x_j . Therefore, a batch of SSL can be viewed as a multi-class classification problem, where each class contains two samples. Then, the training data of n batches of self-supervised learning can form n self-supervised learning tasks. Our framework updates the self-supervised model f_{θ} in GeSSL based on these n tasks simultaneously. Therefore, the number of sampled samples per batch of self-supervised learning directly determines the class diversity of the data in the task. In this section, we conduct ablation experiments on the batch size (the number of classes) of the tasks and the number of self-supervised learning tasks n that are learned simultaneously.

Specifically, we choose the commonly used unsupervised learning benchmark dataset STL-10, semi-supervised learning benchmark dataset ImageNet with 10% label, and the few-shot learning benchmark dataset miniImageNet, and evaluate the performance of SimCLR + GeSSL under different batch sizes and different n values. Figure 7 shows the

impact of different batch sizes (i.e., the number of classes in the multi-class classification task) for SSL. The results show that SimCLR + GeSSL always outperforms SimCLR under any batch size. A larger batch size leads to a slightly larger performance improvement for SimCLR + GeSSL, but also increases the computational resource consumption. Therefore, in this study, we build tasks based on images with a batch size of $B = 16$ or $B = 32$. Figure 8 shows the impact of the update frequency n (i.e., update f_θ every n batches) for the second-level optimization. The results indicate that $n = 8$ is a better trade-off between model accuracy and time consumption. In the setting of our GeSSL, we also choose $n = 8$ as the hyperparameter setting.